Atmos. Chem. Phys. Discuss., 14, 303–375, 2014
www.atmos-chem-phys-discuss.net/14/303/2014/
doi:10.5194/acpd-14-303-2014

Atmospheric Chemistry and Physics Discussions

The effect of solar zenith angle on MODIS cloud optical and microphysical retrievals

D. P. Grosvenor[1,*] **and R. Wood**[1]

[1]Department of Atmospheric Science, University of Washington, Seattle, USA
[*]now at: School of Earth and Environment, University of Leeds, UK

Received: 13 September 2013 – Accepted: 4 December 2013 – Published: 7 January 2014

Correspondence to: D. P. Grosvenor (daniel.p.grosvenor@gmail.com)

Published by Copernicus Publications on behalf of the European Geosciences Union.

Abstract

In this paper we use a novel observational approach to investigate MODIS satellite retrieval biases of τ and r_e (using three different MODIS bands: 1.6, 2.1 and 3.7 µm, denoted as $r_{e1.6}$, $r_{e2.1}$ and $r_{e3.7}$, respectively) that occur at high solar zenith angles (θ_0) and how they affect retrievals of cloud droplet concentration (N_d). Utilizing the large number of overpasses for polar regions and the diurnal variation of θ_0 we estimate biases in the above quantities for the open ocean region north of Scandinavia that is dominated by low level stratiform clouds.

We find that the mean τ is fairly constant between $\theta_0 = 50^\circ$ and $\sim 65^\circ$, but then increases rapidly with an increase of over 70 % between the lowest and highest θ_0. $r_{e2.1}$ and $r_{e3.7}$ decrease with θ_0, with effects also starting at around $\theta_0 = 65^\circ$. At low θ_0, the r_e values from the three different MODIS bands agree to within around 0.2 µm, whereas at high θ_0 the spread is closer to 1 µm. The percentage changes of r_e with θ_0 are somewhat lower than those for τ being around 5 % and 7 % for $r_{e2.1}$ and $r_{e3.7}$. For $r_{e1.6}$ there was very little change with θ_0.

The increase in τ and decrease in r_e both contribute to an overall increase in N_d of 40–70 % between low and high θ_0. We argue that such a change is highly unlikely to be due to any physical diurnal cycle, which is supported by the finding that the retrieved N_d is constant at local times at either side of noon for which $\theta_0 < 65^\circ$. Whilst the overall r_e changes are quite small, they are not insignificant for the calculation of N_d; we find that the contributions to N_d biases from the τ and r_e biases were roughly comparable for $r_{e3.7}$, although for the other r_e bands the τ changes were considerably more important (roughly twice the contribution for $r_{e2.1}$ and six times for $r_{e1.6}$). However, when considering only the clouds with the more heterogeneous tops, the importance of the r_e biases was considerably enhanced for both $r_{e2.1}$ and $r_{e3.7}$; τ and r_e bias contributions were comparable for $r_{e2.1}$ and for $r_{e3.7}$ r_e bias contributions were ~ 50 % greater.

ACPD
14, 303–375, 2014

For a given θ_0, large decreases in r_e were observed as the cloud top heterogeneity changed from low to high values: decreases of 25–30 % for $r_{e3.7}$, ~ 20 % for $r_{e2.1}$ and 10 % for $r_{e1.6}$, although, it is possible that physical changes to the clouds associated with cloud heterogeneity variation may account for some of this. However, for a given cloud top heterogeneity we find that the value of θ_0 affects the sign and magnitude of the relative differences between $r_{e1.6}$, $r_{e2.1}$ and $r_{e3.7}$, which has implications for attempts to retrieve vertical cloud information using the different MODIS bands. The relatively larger decrease in $r_{e3.7}$ and the lack of change of $r_{e1.6}$ with both θ_0 and cloud top heterogeneity suggest that $r_{e3.7}$ is more prone to retrieval biases due to high θ_0 than the other bands, which is interesting since $r_{e3.7}$ has generally been shown to be less prone to other retrieval biases (e.g. due to sub-pixel heterogeneity) at low θ_0. We discuss some possible reasons for this.

Our results have important implications for individual MODIS swaths at high θ_0, which may be used for case studies for example. θ_0 values $> 65^\circ$ can occur at latitudes as low as 28° in mid-winter and for higher latitudes the problem will be more acute. Also, Level 3 daily averaged MODIS cloud property data consists of the averages of several overpasses for the high latitudes, which will occur at a range of θ_0 values. Thus, some biased data is likely to be included.

1 Introduction

The MODIS (Moderate Resolution Imaging Spectroradiometer) instruments onboard the Aqua and Terra polar orbiting satellites are capable of retrieving cloud optical depth (τ) and effective radius (r_e) information from liquid clouds based upon the combination of one non-absorbing optical wavelength (0.86 µm is used by MODIS for retrievals over the ocean) and one absorbing near-infrared band (Foot, 1988; Nakajima and King, 1990; King et al., 1997; Platnick et al., 2003); this can be either 1.6, 2.1, or 3.7 µm. r_e retrieved using these different bands will hereafter be referred to, respectively, as $r_{e1.6}$, $r_{e2.1}$ and $r_{e3.7}$, with $r_{e2.1}$ being the value provided as standard from MODIS (e.g.

ACPD
14, 303–375, 2014

in Level-3 products). This information is invaluable for a range of cloud microphysical studies, especially given the global coverage and the long time period of the dataset available from these instruments (Terra MODIS since mid-2000 and Aqua MODIS since 2002).

Additionally, this information can be used to estimate cloud droplet number concentrations (N_d) within liquid clouds (Boers et al., 2006; Bennartz, 2007, hereafter B07). N_d is a very useful parameter since in non-precipitating clouds it depends mainly upon the concentration of available cloud condensation nuclei (CCN), although to a lesser extent it also depends upon the cloud updraft speed. Thus, for non-precipitating clouds with fixed updraft speeds, N_d is a good indicator of available CCN concentrations. Parameters like r_e alone are not as useful in this regard since r_e is dependent on both N_d and the local liquid water content of the cloud, which may both be variable. This makes an N_d dataset useful for estimates of aerosol indirect effects (AIEs), for example Nakajima et al. (2001) and Quaas et al. (2008). Precipitation can also be an important sink process for N_d and, therefore, insight into such processes can be gained through knowledge of N_d (e.g. Wood et al., 2012).

A global long term dataset of N_d would also allow the evaluation of the representation of AIEs in global models, something that cannot be reliably achieved from ground and aircraft measurements with their generally poor spatial and temporal sampling. The representation of AIEs in climate models is complex and involves interactions between several processes. Thus, simulating it is a strong test for climate models. However, there are large variations of AIE estimates between different climate models (Quaas et al., 2009; IPCC, 2007) demonstrating large uncertainties in the understanding of these processes and therefore large uncertainties in the predicted climate forcing.

Marked differences in predicted N_d also exist between different GCMs, which is a good indicator that models are not correctly capturing the key controls on N_d. This is likely to result in poor prediction of AIEs. Using observations of N_d to evaluate and constrain N_d in models might give insight into how to improve this situation. Additionally, many climate models arbitrarily fix a lower limit for N_d (Hoose et al., 2009; Quaas et al.,

ACPD
14, 303–375, 2014

2009). This has been shown to affect the strength of predicted AIEs across GCMs; in one model removing this limit changed the global AIE by 80 % (Hoose et al., 2009). Satellite based measurements of N_d might represent a way to determine this lower limit (if one exists).

However, there are problems with satellite retrievals and they need to be assessed before a robust and reliable N_d dataset can be produced. This paper aims to examine some aspects of these problems, in particular issues that occur when retrievals are made at high Solar Zenith Angles (θ_0). There have been a number of studies that have examined optical depth artifacts for non-absorbing wavelength retreivals at high θ_0, which will be discussed in Sect. 2.2.1. However, the effect on MODIS retrievals has not been studied, likely due to the difficulty in obtaining an objective test. Here we attempt such a study and extend the analysis to examine issues with r_e and N_d retrievals also.

The paper is organized as follows: Sect. 2 describes the methods, which includes a description of the method used to estimate N_d and a discussion the validity of some of the assumptions required (Sect. 2.1 and Appendix A); a discussion on what is known from the previous literature about the effects of cloud heterogeneity and θ_0 on cloud retrievals (Sect. 2.2); and the method that we use here to estimate the effects of θ_0 on τ, r_e and N_d retrievals (2.3). Section 3 describes the main results, the effect of θ_0 and also the effect of cloud top temperature heterogeneity; Sect. 4 discusses potential causes of the effects observed; and Sect. 5 provides a summary and discusses some of the ramifications of the results for the MODIS dataset.

2 Methods

2.1 The method used to estimate droplet concentration.

The method used for the estimation of N_d from MODIS τ and r_e measurements follows that described in Boers et al. (2006) and B07. Details about this, including necessary assumptions and their justification are discussed in Appendix A. The N_d retrieval

ACPD
14, 303–375, 2014

method is based upon measurements of τ and r_e. We now discuss potential artifacts for these retrievals in some detail since such processes are important in attempting to understand the high θ_0 biases investigated here.

2.2 Potential optical retrieval artifacts

As well as assumptions regarding the vertical structure of the cloud that are necessary to allow the N_d calculation (see Appendix A), we must also consider the assumptions that exist for the MODIS optical retrievals of τ and r_e. A large cause of artifact here is likely due to the use of the plane parallel (PP) radiative transfer algorithm that is used to build look-up tables (LUTs) for converting pairs of non-absorbing wavelength reflectance (R_{nab}) and absorbing wavelength reflectance (R_{ab}) into τ and r_e values (Nakajima and King, 1990). This requires that the clouds are horizontally homogeneous both within a single 1 km × 1 km MODIS pixel and at scales outside of a given pixel. The latter is required because the plane parallel approximation requires that each pixel be unaffected by any other pixel (the Independent Column Approximation, ICA). Under conditions where 3-D radiative transfer of light occurs in a non-homogeneous environment, net horizontal photon transport can occur and thus this assumption breaks down. The assumption of no variability at scales below that of a MODIS pixel (1 km × 1 km) has also been shown to be untrue for real clouds (e.g. Zhang et al., 2012, hereafter Z12). In fact LWC variability of clouds has been shown to extend down to scales smaller than 4 cm (Marshak et al., 1998), although that study suggested that variability below the scale of the mean free path of photons in clouds (~ 10–30 m for stratocumulus) was not important for remote sensing applications

The breakdown of either of these assumptions can lead to biases in the retrieved optical properties, although assessment of the direction and magnitude of these effects is complicated. MODIS optical property retrievals are made using reflectances and the effect of cloud heterogeneity on these depends on the solar and viewing geometry; i.e. upon θ_0, the sensor zenith angle (θ) and on the relative azimuth angle (ϕ). Much more work on the effects on τ than on r_e has been reported. However, any artifacts of the r_e

ACPD
14, 303–375, 2014

retrieval are likely to be important for N_d calculations because of the strong sensitivity of N_d to r_e that is inherent in Eq. (A1).

2.2.1 Optical depth retrieval artifacts

Cahalan et al. (1994) showed that the non-linearity of the relationship between R_{nab} and τ causes a decrease in albedo for heterogeneous clouds compared to a plane-parallel cloud with the same mean τ. This is known as the plane parallel (PP) albedo bias and is likely to lead to τ underestimates made using the measured reflectances and PP LUTs. Also, at near-nadir viewing angles and for low θ_0, cloud variability is known to cause the mean reflectance of a region to be slightly reduced compared to a homogeneous cloud with the same mean τ via 3-D effects, due to the leakage of photons horizontally from the sides of the region and due to channeling of photons from regions of high extinction to regions of low extinction where they can be lost through downward transport (Loeb et al., 1997; Davies, 1978; Kobayashi, 1993; Varnai and Davies, 1999). However, these biases are generally small compared to those that have been reported at high θ_0.

Loeb and Davies (1996) and Loeb and Davies (1997) calculated optical depths (using LUTs generated using the plane parallel approximation) from reflectances obtained from ERBE observations (with resolution of 31 km × 47 km) at various θ_0. Loeb and Coakley (1998) used AVHRR observations (with a resolution of 4 km at nadir, degrading to 13 km at the swath edge) to perform a similar study, but on marine stratocumulus clouds only. The results showed that at high θ_0 ($\theta_0 \gtrsim 65^\circ$) the optical depth inferred from observations increased with θ_0 and this was attributed to the increasing (positive) difference in reflectances between the real observed clouds and those calculated from the PP model as θ_0 increased. The same direction of bias was generally found for both backscattering and forward scattering angles and for a range of θ, suggesting that the θ_0 bias may be present for a range of viewing geometries and not just at nadir. In general, high θ_0 biases for forward scatter were generally greater than those at backscatter for a given θ. The results were found to be very sensitive to the thickness of the cloud with higher biases reported for the more optically thick clouds; for $\tau > 12$ and nadir

ACPD
14, 303–375, 2014

viewing the positive bias was present even at low θ_0. Some dependence of the high θ_0 reflectance bias on θ was found. However, its behavior varied with the cloud thickness. The response to θ in the forward scatter direction was also sensitive to the setup of the PP model.

The conclusions from the above observational studies are, however, reliant on the cloud fields being statistically similar as a function of viewing geometry. They also could not take into account biases present at low θ_0 and low θ since these clouds were used to generate the PP relationship between reflectance and τ. However, this is not a factor for modelling studies where the cloud field is known. Using Monte Carlo 3-D radiative transfer modeling of heterogeneous 35.1 km × 35.1 km cloud fields generated using stochastic methods, Loeb et al. (1997) showed that 3-D nadir reflectances increase with θ_0, whereas reflectances calculated using the PP approximation decrease. This was consistent with the above observational studies indicating that 3-D radiative transfer effects within a heterogeneous cloud environment were the cause. Sensitivity tests suggested a roughly equal contribution to the bias from cloud side illumination effects and cloud top height variability effects, with the latter effect attributed to changes in the slope of cloud elements at cloud top. Note that such effects occurred even for completely overcast scenes. Initially, the cloud field that was generated only contained cloud top height variability; the extinction of the cloud field was held constant. However, adding extinction variability did not have a significant effect. Similar conclusions were found from the modeling results of Varnai and Davies (1999).

One limitation of these modelling studies is that only nadir views were tested and the observational data indicated that both θ and ϕ viewing angles might modulate the τ bias at high θ_0. Liang and Girolamo (2013) also found that τ retrievals are likely to be affected by θ and ϕ by examining MISR retrievals performed at several ϕ. The results of Liang and Girolamo (2013) were all relative to the nadir view value and thus they could not assess how much the nadir view τ itself was changing with θ_0. The effects were observed to be complicated and the sign and magnitude of the nadir relative biases was suggested to be dependent upon many competing factors. It was also found

ACPD
14, 303–375, 2014

that cloud heterogeneity tended to enhance the magnitude of the effects, particularly for low optical depth clouds and at high θ_0. However, significant τ biases were generally not seen until very high θ values of 70.5° were reached; biases within the MODIS θ range were much lower. Also, for the cloud scenes sampled ϕ generally changed from near 0° to near 90° with increasing latitude. This meant that θ_0 varied in tandem making it difficult to separate the two effects.

Finally, Seethala and Horvath (2010) found that MODIS derived LWP measurements increased significantly relative to co-located measurements from AMSRE (Advanced Microwave Scanning Radiometer-EOS) at high θ_0. A large part of this was attributed to unphysical increases in τ with θ_0. The increase was greater as the inhomogeneity of MODIS τ over the 0.25° × 0.25° scenes increased, which is consistent with the above results.

2.2.2 Effective radius retrieval artifacts

Whilst there have been a number of studies examining the effects of cloud variability and viewing geometry on τ retrievals there have been far fewer studies on the r_e effect. Marshak et al. (2006, hereafter M06) was one of the first to do so and introduced a theoretical basis to attempt to explain the effects of 3-D radiative transfer on r_e retrievals that were made using cloud fields from an LES model. M06 divided the effects into those due to resolved variability of reflectances (i.e. variability at scales larger than the satellite pixel size) and those due to sub-pixel scale variability. In both cases it was assumed that the τ and r_e retrievals were independent; i.e. for the r_e retrieval it was assumed that τ variability did not affect the relationship between r_e and reflectance in the absorbing band (R_{ab}). Similarly it also means that only the non-absorbing reflectances (R_{nab}) need to be considered to determine τ.

M06 used the idea of "shadowing" and "brightening" caused by 3-D radiative transfer. Shadowing refers to pixels for which the reflectance is decreased from the PP value due to 3-D effects and brightening to pixels for which the reflectance is increased. An estimate of the resolved scale effect was made for an equal number of shadowed and

ACPD
14, 303–375, 2014

brightened pixels for which the magnitudes of shadowing and brightening were the same. In that case, 3-D radiative transfer effects were expected to lead to a tendency for an overall increase in r_e and τ (relative to the true values) due to the non-linearity of the relationship between the reflectances and r_e and τ. However, it was noted that in reality there are unlikely to be equal numbers of shadowed and illuminated pixels (of a given magnitude of shadowing/brightening) since this would require that there be no overall reflectance change due to 3-D effects. The works cited in the previous section (2.2.1) suggest that this is unlikely to be the case, at least for R_{nab}. Additionally, the assumption of independent τ and r_e retrievals is unlikely to hold true since the MODIS LUTs used to convert reflectances into τ and r_e are 2-D in nature, and are non-orthogonal in the regions corresponding to low τ (Nakajima and King, 1990, see their Fig. 2). In such regions it is likely necessary to consider the simultaneous variations of reflectances in both bands, which essentially equates to simultaneous variations in r_e and τ. Nevertheless, the results from the retrievals made from reflectances calculated from the LES cloud model fields corroborated the theoretical argument, suggesting that, at least in this case, the assumptions may have been valid, or irrelevant.

The conceptual model of M06 suggested that sub-pixel variability would lead to a low bias of both the τ and r_e values retrieved for that pixel due to averaging of the reflectances prior to the retrieval of τ and r_e (a satellite viewing the pixel would report the averaged reflectance). The assumption of independence of the τ and r_e retrievals can be questioned in this case too. Again, though, the results from the LES model retrievals in M06 corroborated the theoretical result, indicating that the assumption may have been valid in the case of this simulation. However, also using retrievals performed on LES clouds Z12 found the opposite result for the effect of sub-pixel averaging of reflectances, with the retrieved r_e increasing above the true sub-pixel r_e mean. Within 800 m × 800 m regions (close to the size of a 1 km × 1 km MODIS pixel) it was found that the r_e of the 100 m × 100 m model resolution elements was approximately constant, but that there was quite a wide spread in τ. Z12 showed that for such variability the nature of the dual-band (i.e. 2-D) LUT used for MODIS retrievals would lead to increases in

ACPD
14, 303–375, 2014

r_e (and decreases in τ) and that the increase would be greater as the sub-pixel heterogeneity of R_{nab} increased. Greater τ variation than r_e variation at scales smaller than a standard MODIS pixel was also demonstrated in Z12 from MODIS observations of real clouds using a 500 m resolution MODIS research algorithm to look at the normalised standard deviations of τ and r_e for a MODIS cloud scene. Whether this is generally true over all cloud scenes is not clear. For the cases considered, these results negated the assumptions of the theoretical basis introduced in M06 since the sub-pixel τ variability meant that the non-orthogonal regions of the LUT were utilized. Thus it remains to be explained why the results from the LES model simulations in M06 were consistent with that theoretical basis.

One major difference between the simulations of M06 and Z12 that might provide a potential explanation is that the radiative transfer on the cloud fields from the M06 simulations were performed at the moderately high θ_0 of 60°, whereas in Z12 radiative transfer was performed at θ_0 = 20 and 50° and on the whole results were reported for the combination of the two θ_0 values. It is likely that the result obtained will depend on the degree of sub-pixel variation of both R_{nab} and R_{ab}, the region of the LUT covered by the reflectance values and the influence on the sub-pixel reflectances of 3-D effects. Such factors are likely to be affected by the value of θ_0. Other factors that alter the orthogonality and non-linearity of the LUTs are also likely to affect this result, such as the near-infrared wavelength used, as also demonstrated in Z12. Their results showed that the increase of r_e due to sub-pixel averaging was substantially greater for the 2.1 µm band relative to the 3.7 µm band, and that this most likely because the LUT for the latter is more orthogonal than for the former.

There have been several attempts in the literature to use the differences between r_e from the different MODIS bands to infer information about the vertical structure of the cloud. This may be theoretically possible since the different wavelengths of light have different penetration depths into the cloud and thus produce a weighted mean r_e that is representative of different vertical regions of the cloud (Platnick, 2000). How-

ACPD
14, 303–375, 2014

ever, the heterogeneity effects just mentioned will clearly impact such attempts. Further discussion on this is deferred to Sects. 3.2.2 and 4.3.

2.2.3 Measures of cloud heterogeneity

Given the sensitivity of the cloud optical retrievals to cloud inhomogeneity it is desirable to restrict them to regions that are as homogeneous as possible. It seems that restricting analysis to regions where the MODIS cloud fraction is high is one way to increase the probability of homogeneity, since it was shown by Wood and Hartmann (2006) that, over the scale of ∼ 200 km, cloud fraction is strongly correlated with a measure of homogeneity based on the MODIS liquid water path (denoted γ_{LWP}). However, the degree of variability at scales smaller than the MODIS 1 km × 1 km pixel size was not assessed. Additionally, it has been shown that inhomogeneities within completely overcast stratocumulus may still introduce retrieval artifacts (Loeb et al., 1997).

PZ11 restricted their analysis to regions that had cloud fractions > 90 % over a 5 km × 5 km region (N.B., the 5 km × 5 km cloud mask is a standard MODIS product). Using another metric, the sub-pixel heterogeneity index, defined in Zhang and Plantnick (2011) as the ratio between the spatial standard deviation and mean of the 0.86 µm reflectance over an area of 1 km × 1 km, PZ11 found that such > 90 % cloud fraction regions were generally very homogeneous by this measure. However, this quantity only measures the sub-pixel scale variability of the clouds. Variability over larger scales was not examined in PZ11 and open questions remain concerning the scale over which homogeneity is required in order to avoid 3-D radiative biases (within acceptable tolerances).

In line with other studies, PZ11 found that, on average, MODIS r_{e} values were 15–20 % too large compared to the in-situ observations, despite the reported sub-pixel homogeneity. The reason for this discrepancy was not established, although it can be speculated that a combination of the types of effects discussed above (3-D radiative transfer and sub-pixel averaging of reflectances) may be to blame. The results also suggest that ensuring low sub-pixel R_{nab} heterogeneity does not mean that r_{e} biases will be avoided.

ACPD
14, 303–375, 2014

Following Cahalan et al. (1994), Seethala and Horvath (2010) assessed cloud homogeneity from MODIS scenes over larger scales ($0.25^\circ \times 0.25^\circ$) using a measure of τ variability (denoted γ_τ). However, a difficulty with the measures of cloud heterogeneity mentioned so far is that they depend on reflectance variability. Variability in reflectance has been shown to be caused by viewing geometry variations (particularly due to high θ_0) and so this is not always a measure of actual physical cloud variability; it is useful to be able to separate these two effects.

In this paper we use the standard deviation of the MODIS Cloud Top Temperature (CTT) over a $1^\circ \times 1^\circ$ region, σ_{CTT}, to characterize heterogeneity. This will not be affected by optical artifacts, as would be the case for γ_τ and γ_{LWP} and thus should be more representative of the physical cloud heterogeneity. This measure also has the advantage that it will characterize cloud top heterogeneites, whereas the other measures could also be affected by e.g. extinction variability within cloud; the studies mentioned in Sect. 2.2.1 (Loeb et al., 1997; Varnai and Davies, 1999) found that cloud top height variability had a larger effect on cloud reflectance than did extinction variability. However, σ_{CTT} may not represent the heterogeneity well if the important scale of variability is at a scale smaller than that of the MODIS CTT resolution (5 km).

2.3 Method for assessing the effect of Solar Zenith Angle on MODIS cloud retrievals

The operational MODIS Level-3 (hereafter L3) dataset is produced by averaging individual Level-2 (L2) swaths onto a $1^\circ \times 1^\circ$ grid on a daily basis. MODIS swaths from individual satellites (i.e. Terra or Aqua) start to overlap at latitudes higher than 23°, which means that some locations at such latitudes are sampled on more than one consecutive overpass. At latitudes higher than 62° three consecutive overpasses are possible and near the poles overpasses occur throughout the day. More than one daylight overpass for a given location means that retrievals are made at more than one local time and therefore with more than one value of θ_0.

ACPD
14, 303–375, 2014

As an example, Fig. 1a and b show the maximum θ_0 of all of the available MODIS Terra (equator crossing time 10:30 LT) and Aqua (13:30 LT) daytime overpasses for 20 June 2007. The results for Terra and Aqua are very similar. Daytime overpasses are defined as $\theta_0 \leq 81.4^\circ$, which is the θ_0 range for which optical retrievals are made (τ, r_e, N_d, etc.). At high southern latitudes there is no data because θ_0 never reaches below this value on this austral mid-winter day. The individual swaths, with data gaps in between at low latitudes, can be discerned from this figure. It also demonstrates the variety of maximum θ_0 values at a given latitude due to the differing number of orbit overlaps that are possible. At low latitudes lower θ_0 values are present towards the eastern (western) regions of the swaths for Terra (Aqua) since these off-nadir regions are sampled at later local times, which are closer to noon relative to the western (eastern) parts of the swaths.

At high northern latitudes the pattern becomes more complicated due to there being several overpasses per day with $\theta_0 < 81.4^\circ$. The exact number varies with longitude as well as latitude, since it depends on how many of the swaths overlap. Figure 1c and d show the difference between the maximum and minimum θ_0 for the same day. From this pattern the changes in the number of overpasses per day can be discerned. North of 62° N the maximum minus minimum θ_0 can reach between ~ 20–45° showing that even though the maximum θ_0 is high there will be some overpasses with a more reasonable θ_0 akin to those sampled at much lower latitudes. The pattern changes from day to day as the centres of the swath paths precess to different longitudes over a 16 day period.

For high latitude regions very high θ_0 retrievals are made. Data from all available overpasses are averaged into a daily value for the Level-3 product, which gives the potential for the inclusion of higher θ_0 retrievals than are necessary and may lead to biases in the retrieved τ, r_e and N_d values, for the reasons discussed earlier. However, the effect of θ_0 on r_e and N_d retrievals remains unquantified and a demonstration of the effect of using actual MODIS data is also lacking. Here we make such an estimate.

ACPD
14, 303–375, 2014

2.3.1 MODIS data employed

Determining the effect of θ_0 on MODIS retrievals using the MODIS data record without also aliasing change in other variables is difficult. At latitudes lower than around 62° there are a maximum of two Aqua or Terra overpasses in daylight hours and thus relatively little θ_0 range is sampled during one day for a given location. To test a wide range of θ_0 for lower latitudes therefore requires that either a long time period is sampled in order to incorporate seasonal changes in θ_0, or that a range of latitudes is sampled. Unfortunately both of these are likely to also cause systematic (but unquantified) changes in N_d due to real-world (i.e. non-retrieval based) changes.

Sampling at higher latitudes, however, offers a solution, although there are limitations there too. Because Aqua and Terra are polar orbiters, at a high enough latitude there will be overpasses throughout the day, which will encompass a wide range of θ_0 values. Unfortunately, throughout most of the year the Sun is too low in the sky to get a low enough minimum θ_0 to allow a wide range of θ_0 values to be tested. However, at mid-summer it is possible to achieve minimum θ_0 values as low as 45° at latitudes as high as 70° and thus a reasonable range of θ_0 can be sampled.

A problem with high latitudes, though, is the presence of ice covered surfaces. Retrievals over ice are generally considered problematic (King et al., 2004) and it is possible that this would introduce its own biases. The Antarctic continent covers most longitudes at the relevant latitudes in the Southern Hemisphere and in regions where that is not the case there is sea-ice present in mid-summer. However, in the Northern Hemisphere the Barents and Norwegian Seas are relatively sea-ice free for most of the year (Fig. 2) and it is here (in the boxed region of the figure) that we focus our efforts.

The period of 13–30 June was chosen for this study in order to allow for a full cycle of the 16 day orbital path precession of the Aqua and Terra satellites and to allow a variety of solar and sensor zenith angle combinations for a given location. However, the period is likely short enough that there would be little seasonal variation in the daily mean θ_0, which is also aided by the choice of a mid-summer time period. Seasonal changes

ACPD
14, 303–375, 2014

are much smaller than the changes in θ_0 due to the diurnal sampling by MODIS. This period is analysed for the years 2007–2010 for both the Aqua and Terra satellites.

When trying to discern the effects of θ_0 on N_d it is important to sample only a small range of latitudes since θ_0 is a strong function of latitude and N_d also may systematically change with latitude. Therefore this would produce spurious results. Thus, the box shown in Fig. 2 was chosen to cover a small latitude range of only 72–75° N. A fairly large longitude range (−3 to 48° E) is chosen to give lower statistical noise. θ_0 values for MODIS overpasses do not vary systematically with longitude and so regional cloud properties should not introduce any apparent θ_0 effects. In order to asses potential longitude dependent or regional effects, we have investigated the effect of splitting the domain into equal sized eastern and western regions and found that the results (shown later) are very similar for both regions. Also, similar results are obtained for both the first half and the second half of the time period. θ and ϕ can both co-vary with θ_0 and certain ranges of both are known to introduce biases in MODIS cloud optical property retrievals as discussed in Sect. 2.2.1. However, we will show shortly that it is possible to isolate the effects of θ_0 and θ.

Apart from the effects just mentioned, the only remaining likely source of systematic variation in cloud properties with θ_0 (apart from the unidentified radiative sources that lead to retrieval errors that we are looking for) is that due to diurnal variation. Since we are utilizing the diurnal variation in θ_0 we cannot remove any potential artifacts due to this. However, we argue that the effect of the diurnal cycle on our results is likely to be small. For brevity, a detailed discussion of this issue is deferred to Appendix B.

2.3.2 Methodology for the MODIS data processing

In a similar manner to that used to create the MODIS L3 product (King et al., 1997; Oreopoulos, 2005), we processed the sub-sampled joint-L2 swaths for these times into $1^\circ \times 1^\circ$ grid boxes. To confirm that there is no effect from the sub-sampling inherent in the joint-L2 product, we also performed the analysis using full resolution L2 files for

ACPD
14, 303–375, 2014

only one of the years and found little change to the results, consistent with Oreopoulos (2005).

Unless otherwise mentioned, for the MODIS dataset referred to throughout the rest of this paper we have applied some restrictions to each $1^\circ \times 1^\circ$ gridbox in order to attempt to remove artifacts that may cause biases:

1. At least 50 joint-L2 1 km resolution pixels from the MODIS swath fell within the gridbox. This represents approximately a third of the total possible for gridboxes at these latitudes.

2. At least 90 % of the available pixels were successfully designated as either liquid cloud, ice cloud, undetermined cloud, or as clear by the MODIS operational optical cloud properties retrieval algorithm and did not suffer from sunglint. For the other 10 % of pixels there was either sunglint, or the MODIS algorithm could not set them as clear or cloudy, which could be due to various factors. Analysis was not performed on such pixels.

3. All of the pixels remaining after restriction (2) were required to be of liquid phase. Thus the liquid cloud fraction over the gridbox (CF_{liq}) was at least 90 %. A high cloud fraction helps to ensure that the clouds are not broken (except for the possibility of clear regions in the 10 % mentioned in (2) and sub-pixel clear regions), since broken clouds are known to cause biases in retrieved optical properties due to photon scattering through the sides of clouds. Often retrievals of droplet concentrations, which rely on optical depth and effective radius, are restricted to high cloud fraction fields for this reason (B07; PZ11) and so we focus on such datapoints here. However, an overcast grid box still allows cloud heterogeneities caused by variations in cloud top height, cloud optical extinction (including sub-pixel scale holes), cloud depth, etc. Thus homogeneity is not ensured. Such issues are discussed in detail in Sect. 2.2.

4. For at least 90 % of the pixels remaining after (3) successful simultaneous retrievals of both τ and r_e were performed and the cloud water path confidence

ACPD
14, 303–375, 2014

from the MODIS L2 quality flags was designated as “very good confidence” (the highest level possible).

5. The mean CTT is restricted to values warmer than 268 K. The reasons for this are discussed shortly.

The restriction to high CF_{liq} also serves the purpose of attempting to ensure that grid boxes with a significant ice cloud fraction are not sampled. However, since MODIS is likely to determine the phase of only the upper regions of the cloud it is possible that the clouds contain ice in their lower regions. Indeed, it has been observed from ground based measurements that Arctic clouds are can be dominated by liquid in their upper regions, but precipitate snow (Morrison et al., 2012). Whether such clouds would be identified by MODIS as being liquid or ice and whether the presence of ice lower in the cloud would affect MODIS retrievals of τ, r_e and N_d are open questions. However, the presence of ice is by no means guaranteed, especially at temperatures closer to 0 °C where ice nuclei concentrations are likely to be very low (DeMott et al., 2010). Ground measurements show that at temperatures warmer than around −5 °C Arctic stratus clouds can, depending on location, be almost completely dominated by liquid (de Boer et al., 2011). Issues regarding the likelihood of the presence of ice are discussed further in Appendix C.

3 Results

3.1 Examining the properties of the sampled clouds

We first examine the distribution of cloud fraction vs. height within the specified region using the CALIPSO GOCCPv2.1 (Chepfer et al., 2010) dataset. (Fig. 3). These data are for the month of June for the period 2007–2010. Here it needs to be borne in mind that CALIPSO can observe clouds at multiple heights within one profile, although thick clouds will rapidly attenuate the signal. CALIPSO reveals the presence of a significant

ACPD
14, 303–375, 2014

number of high level clouds although the mode height is 0.48–0.96 km. Thus there are a lot of clouds that likely reside within the boundary layer and which would therefore be well suited to the application of the N_d estimate using MODIS, as described in Sect. 2.1 and Appendix A.

Figure 3b shows PDFs of MODIS gridbox mean CTT for low and high θ_0 cases for grid boxes with restrictions (1–4) applied. The PDFs reveal that for both low and high θ_0 almost all of these datapoints have CTTs warmer than 260 K with a mode at around 269 K. Thus, the majority of the clouds have subzero CTTs, which may allow for some ice formation. However, as discussed above and in Appendix C, ground based observations in the Arctic generally indicate a dominance of liquid or mixed phase clouds for such cloud top temperatures.

For the low θ_0 data there is an interesting secondary mode at around 264 K, which is not present for high θ_0. Although this could indicate physical differences between the low and high θ_0 clouds (e.g. fewer liquid cloud tops at high θ_0 at the colder temperatures, perhaps related to a reduction in cloud top SW heating), the difference seems more likely to be due to retrieval differences, since if restrictions (3) and (4) are lifted the low and high θ_0 CTT PDFs are almost identical (not shown).This indicates a difference between the number of pixels that are determined to be liquid at low and high θ_0, despite having the same CTT distribution for the general unscreened population. A change in cloud glaciation due to a reduction in SW heating at high θ_0 might be expected to be accompanied by changes in CTT. Further, there are more pixels classified as "undetermined" phase at high θ_0, which also points towards problems with the phase determination being the cause. Because of the differences in CTT PDFs at CTT $<\sim$ 268 K and given the increased likelihood of ice at such temperatures a further restriction (5) is thus applied to limit CTT to values warmer than 268 K.

Figure 4 shows the number of $1^\circ \times 1^\circ$ datapoints for each pairing of sensor (θ) and solar zenith angles (θ_0) for the dataset following the application of restrictions 1–5. The figure reveals that between θ_0 of $\sim 55^\circ$ and 67° there is a only a narrow range of θ encompassing only values $> 50^\circ$. For $\theta_0 < 52.5^\circ$ and $\theta_0 > 72.5^\circ$ a spread across almost

ACPD
14, 303–375, 2014

all possible θ values is sampled. This will allow the testing of the θ_0 effect in isolation of potential effects due to a high θ. It also shows that restricting the maximum θ of MODIS L3 datapoints would not be enough to avoid all high θ_0 data being included. The sampled ϕ (not shown) all correspond to angles within 30° of side scattering (= 90°), comprising two narrow ranges: 65–72.5° and 112.5–120°. Thus, the variability of ϕ is unlikely to greatly affect the results.

3.2 Cloud properties vs. θ_0

We now show results of averages over the whole domain and time period of various retrieved microphysical cloud properties in different solar zenith angle bins. The results are split into averages for data in which θ was $\leq 41.4°$ and for $> 41.4°$ to isolate the effects of θ_0 from those of θ. 41.4° is chosen since this represents the halfway point of $\cos(\theta)$ between 0° and the maximum MODIS θ of 60°. It has also been shown that a higher θ results in an increase in the reported MODIS cloud fraction (Maddux et al., 2010). This was thought to have been due to lower instrument resolution and an increased path length between the scene and the satellite with increasing θ, both of which make cloud detection more likely.

In subsequent plots, error bars represent the combined (in quadrature) instrument and sampling errors. L2 MODIS uncertainties in τ and r_e (as provided with the retrievals) are averaged (using a simple mean) to produce $1° \times 1°$ uncertainties. This therefore assumes that L2 pixel uncertainties are fully correlated within each L3 box ($1° \times 1°$), which is also the case for the operational L3 uncertainty estimate. However, when calculating the domain and period mean values from $1° \times 1°$ boxes the instrument uncertainties are combined in quadrature assuming no correlation in order to assess the magnitude of random instrument errors. Departures outside of the calculated error range are therefore likely to represent a systematic bias. Sampling errors are calculated based on the standard deviation of the quantity of interest and the number of samples within each bin.

ACPD
14, 303–375, 2014

3.2.1 Optical depth

Figure 5 shows the mean optical depth in each SZA bin. At intermediate θ_0, only $\theta > 41.4^\circ$ data is available and for the θ_0 bin centered near to 75° only data for $\theta < 41.4^\circ$ is available. This is due to the sampling pattern of MODIS (as demonstrated in Fig. 4).

Mean τ values are very similar for the two θ ranges at both low θ_0, and for the θ_0 bin centered around ~ 71°. For the 79.1° bin the τ value for high θ is 14 % larger than that for low θ. Although the error associated with the high θ value in this θ_0 bin is fairly large, this might indicate a dependence of τ on θ at very high θ_0, although it is also possible that the tendency to observe a higher cloud fraction at high θ could also be having an influence on the identification of scenes with cloud fraction > 90 %.

The high θ results show that τ is fairly constant up to a θ_0 value of approximately 65°. It is speculated that this would also have been the case for low θ retrievals if they had been made. For both low and high θ the τ values at the highest θ_0 are higher than those at the lowest θ_0. The relative increases in τ between the lowest and highest θ_0 bins were 70 and 92 % for the low and high θ cases, respectively (see Table 2; this table also contains these values for r_e and N_d), representing very large increases in τ due to increasing θ_0. Figure 7 shows PDFs of τ at low (50–55°) and high (75–81°) θ_0 ranges for low θ only. The distribution shape is approximately lognormal in both cases and is essentially just shifted towards higher values in the high θ_0 case; Table 1 gives the mean τ values and the normalized standard deviations.

3.2.2 Effective radius

For r_e the results are more complicated (Fig. 6a). Here results from the three different MODIS retrieval wavelengths for r_e are shown ($r_{e1.6}$, $r_{e2.1}$ and $r_{e3.7}$). The standard MODIS wavelength is 2.1 µm and r_e errors are only available for this band. Therefore, the percentage errors for this wavelength are applied as errors for the other wavelengths to give an estimate of the expected uncertainty.

ACPD
14, 303–375, 2014

For the 2.1 and 3.7 µm bands there is a decrease in the mean r_e between the lowest and highest θ_0 bins. This is also evident in the PDFs in Fig. 8 (low θ only), which show a shape close to a normal distribution. The individual changes between the two ranges of 50–55° and 75–81° are listed in Table 2 for both low and high θ; for $r_{e2.1}$ there is a mean decrease of 5 % for low θ and 8 % for high θ, whereas for $r_{e3.7}$ the corresponding decreases are 7.4 % and 8.7 %. The decreases are much smaller for the 1.6 µm band, being only 1.1 and 1.6 % for the low and high θ ranges, respectively. Thus in all cases there is a slightly larger decrease at high θ than at low θ. The high θ results that span the θ_0 range between 51.5° and 71.5° suggest a lack of dependence on θ_0 in this range, which is similar to the τ result.

For a given θ range there is generally very good agreement between $r_{e1.6}$, $r_{e2.1}$ and $r_{e3.7}$ for the lower θ_0 values. At θ_0 of ~ 71° and above, the spread between the different r_e values increases with the largest spread being at the highest θ_0 value tested. At this θ_0, $r_{e3.7} < r_{e2.1} < r_{e1.6}$ for a given θ range. This is the opposite of what would be expected from a cloud in which the LWC was increasing with height adiabatically given the different penetration depths of the different light wavelengths (Platnick, 2000). However, this is in concurrence with several other works that have investigated MODIS retrievals such as Zhang and Plantnick (2011) and Seethala and Horvath (2010). Discussion on the possible reasons for this is deferred to Sect. 4.3.

3.2.3 Droplet concentration

Droplet concentrations calculated from the 1° × 1° mean τ and mean r_e using Eq. (A1) are shown in Fig. 6b as a function of θ_0. The mean τ and r_e are used rather than the individual 1 km values to be consistent with previous estimates that use Level-3 data and to reduce errors that may be caused by high resolution point estimates. For both the 2.1 and 3.7 µm bands mean r_e values were shown to decrease with θ_0 and τ was shown to increase. Therefore, it is perhaps not a surprise that N_d increases with θ_0 given Eq. (A1). N_d also increases with θ_0 for the 1.6 µm band where the r_e decreases were much smaller. This suggests that the increase in τ is dominating the

ACPD
14, 303–375, 2014

N_d increase in that case, although it is possible that changes in the spread of the r_e size distribution and/or negative correlation between τ and r_e could also be playing a role. Issues regarding the relative roles of these factors in causing the changes in N_d with θ_0 are discussed in Sect. 3.5.

Figure 9 shows PDFs at low and high θ_0 (for low θ only) and reveals approximately lognormal shapes. For low θ, the increases in N_d between low and high θ_0 were 39 %, 48 % and 51 % for the 1.6, 2.1 and 3.7 µm bands; for high θ the corresponding increases were 47 %, 65 % and 68 %. In addition, the low θ values are higher than the high θ ones for all wavelengths and at all θ_0. For the highest θ_0 this result is inconsistent with the τ result whereby higher τ values occurred for higher θ. This suggests that the decrease in r_e with increasing θ is dominating at high θ_0. Again, further discussion of such issues is deferred to Sect. 3.5. In a similar manner to τ and r_e there is a change in the behaviour of N_d at a θ_0 value of around 65° with little dependence upon θ_0 for $\theta_0 < 65°$.

3.3 The diurnal cycle

In Sect. 2.3.1 and Appendix B we discussed the potential of a real (i.e. physical) diurnal cycle of the stratocumulus clouds causing apparent effects due to θ_0. It was noted that for the area concerned O'Dell et al. (2008) reported LWP diurnal amplitudes of $<\sim$ 10–20 %. If adiabatic clouds with no diurnal cycle in N_d are assumed then this was shown to translate to a τ diurnal amplitude of 8–17 % and an r_e amplitude of 1.5–3 %. Plotting N_d against local time of day (Fig. 10) instead of θ_0 indicates that there is very little diurnal cycle in N_d because N_d values are almost constant between the hours of $\sim$ 7 and 18:00 LT when using $r_{e2.1}$ and $r_{e3.7}$. If there was a diurnal cycle in N_d then some variation would be expected. These times correspond to those for which θ_0 is $<$ 63–67°, which is consistent with our results in the previous sections that showed θ_0 effects for $\theta_0 \gtrsim 65°$. The symmetry of the lines around local noon also suggests an effect due θ_0 artifacts rather than a physical diurnal effect since the observed LWP diurnal cycle

ACPD
14, 303–375, 2014

was shown in O'Dell et al. (2008) to be asymmetrical with a maximum value at around 03:00–06:00 LT.

The results for effective radius (not shown) for $r_{e2.1}$ and $r_{e3.7}$ are very similar to those of N_d. Those for τ (not shown) do show some asymmetry around local noon that would be consistent with a real diurnal cycle. However, the observed increase in τ of 70–90 % at high θ_0 relative to at low θ_0 is much larger than the expected 8–17 % increase in τ due to the LWP diurnal cycle. However, it is difficult to estimate the true τ diurnal cycle from our results and therefore to fully resolve the effects seen here into those due to θ_0 artifacts and those due to any real diurnal cycle. Therefore, this is left to future work. Another remaining issue is that the diurnal results using $r_{e1.6}$ were more complicated than those of $r_{e2.1}$ and $r_{e3.7}$ suggesting the potential for either height (within cloud) dependent effects or the possibility that retrievals from this band are less reliable. The work required to solve these issues is also beyond the scope of this paper.

3.4 The effect of cloud heterogeneity

Figure 3c shows PDFs of σ_{CTT} for gridboxes that have had restrictions (1–5, see Sect. 2.3.2) applied and for $\theta \leq 41.4^{\circ}$ for both low and high θ_0. The distributions at low and high θ_0 are very similar suggesting that the variability of cloud top height is comparable when the Sun is oblique (i.e. near sunrise/sunset) and when it is higher in the sky (near local noon), at least for this restricted subset of clouds and at the scales probed by the 5 km resolution CTT measurements. This indicates that the diurnal cycle is having little physical impact on this aspect of cloud heterogeneity. Therefore we might expect that for a given σ_{CTT}, the subsets of clouds at low and high θ_0 are likely to be physically similar in this respect, so that any differences in the retrieved τ and r_e are primarily due to retrieval artifacts.

We now examine the variation of τ, r_e and N_d as a function of σ_{CTT}. The restrictions 1–5 described in Sect. 2.3.2 still apply for these results.

ACPD
14, 303–375, 2014

3.4.1 Cloud heterogeneity effects on optical depth

Figure 11a shows mean τ as a function of σ_{CTT}, at low θ values of $< 41.4^{\circ}$ for both low and high θ_0. Figure 11b shows the τ difference between high and low θ_0 vs σ_{CTT}. In the lower range of σ_{CTT} ($<\sim 0.625$–0.875 K) τ increases as σ_{CTT} decreases for both low and high θ_0. The increase is much larger for high θ_0 (58 % increase between $\sigma_{CTT} = 0.875$ and $\sigma_{CTT} = 0.125$ K) than for low θ_0 (an increase of 27 % over the same range). At higher σ_{CTT}, τ is approximately constant within the error range. It is evident that the increase in τ between low and high θ_0 occurs at all values of σ_{CTT}. However, the increase is greatest at low values of σ_{CTT}, i.e. when the cloud tops are more homogeneous.

These results are surprising as previous work (Loeb et al., 1997; Varnai and Davies, 1999) has suggested that a "bumpy" cloud top was the most likely explanation for the increase in τ with increasing θ_0. If that were the case then it might be expected that τ would increase with increasing σ_{CTT} at high θ_0, that the τ increase with θ_0 would be greater at higher σ_{CTT}, and that at low σ_{CTT} there would be little difference in τ between low and high θ_0 cases. This suggests that either: (1) σ_{CTT} is not an appropriate indicator of cloud top heterogeneity in terms of producing τ retrieval artifacts for these clouds. A possible reason for this could be that, as mentioned earlier, the spatial scale of the cloud top variations that cause the increase in τ is smaller than what can be resolved by the 5 km resolution available from MODIS CTT data. However, it seems likely that small scale variability would also increase in conjunction with increases in the variability at scales resolved by the 5 km CTT data; (2) another form of heterogeneity is the cause. Extinction variations inside the cloud (without cloud top height variability) is one possibility, although this was found to have a small effect in Loeb et al. (1997) and Varnai and Davies (1999). Sub-pixel variability is another likely factor. This was suggested to cause τ decreases in M06 and Z12 and so this my be counteracting the expected increase due to resolved scale heterogeneity; or (3) that the actual (i.e. as opposed to the retrieved) τ of the clouds was lower at higher σ_{CTT}. The physically

ACPD
14, 303–375, 2014

higher τ values at low σ_{CTT} might be expected to lead to a greater τ bias between low and high θ_0 (Loeb and Davies, 1996, 1997; Loeb and Coakley, 1998), as seen in Fig. 11.

Further analysis of the relative merit of these explanations is beyond the scope of this study.

3.4.2 Cloud heterogeneity effects on effective radius

Figure 12a and b show r_e for the different wavelengths vs. σ_{CTT} at low and high θ_0, respectively. The figure shows r_e values that decrease with increasing σ_{CTT} (i.e. increasing cloud top heterogeneity) for all wavelengths. However, $r_{e3.7}$ experiences the largest decrease and $r_{e1.6}$ experiences only small changes. At low σ_{CTT}, $r_{e3.7} > r_{e2.1} > r_{e1.6}$, which is actually what would be expected given the increased penetration depth of the shorter wavelength bands relative to the longer wavelength ones and an assumed increase of droplet size with height (e.g. see Platnick, 2000). The contrast to the usual MODIS observation of $r_{e3.7} < r_{e2.1} < r_{e1.6}$ (e.g. Zhang and Plantnick, 2011) raises the possibility that the latter is caused by cloud top heterogeneity and that for homogenous cloud tops (at low θ_0) the r_e retrievals are more reliable and less prone to artifacts. Again, though, we have to bear in mind the possibility of physical cloud changes with σ_{CTT}.

The high θ_0 results follow a similar pattern with a larger r_e decrease with increasing σ_{CTT} for $r_{e3.7}$ and $r_{e2.1}$ compared to $r_{e1.6}$. In fact, in the lower range of σ_{CTT} (< 0.6 K) $r_{e1.6}$ actually increases slightly with σ_{CTT}. The convergence of $r_{e1.6}$, $r_{e2.1}$ and $r_{e3.7}$ at the lowest σ_{CTT} value is probably fortuitous and likely due to the trends with σ_{CTT} of the different wavelength r_e values. Such convergence also occurs in Fig. 12a, although at a higher σ_{CTT} value. The difference can likely be put down to the effect of θ_0 since Fig. 3c suggests that the low and high θ_0 clouds would be physically similar at a given σ_{CTT}.

Additionally, the r_e values at high θ_0 are generally lower than, or similar to, those at low θ_0 for any given σ_{CTT}, with the differences being considerably greater for $r_{e3.7}$ and

ACPD
14, 303–375, 2014

$r_{e2.1}$ than for $r_{e1.6}$. The relative lack of change of $r_{e1.6}$ with θ_0 and σ_{CTT} again raises the possibility that this wavelength might be less susceptible to r_e artifacts caused by cloud top heterogeneity at high θ_0. It also might be an argument against physical droplet size variations with σ_{CTT}. On the other hand, the overall reliability of MODIS r_e retrievals using the 1.6 µm band is still a matter of debate. For the other wavelengths, the decreases in r_e between low and high σ_{CTT} are large, with the maximum decrease being 4.3 µm (35 %) in the case of $r_{e3.7}$ at high θ_0. Given the sensitivity of N_d to r_e this is likely to have a large impact on the retrieved N_d.

3.4.3 Cloud heterogeneity effects on droplet concentration

Similar plots to Fig. 12, but for N_d, are shown in Fig. 13a and b. Interestingly, in the low θ_0 case, at low σ_{CTT}, N_d values for all 3 wavelengths are very similar and there is little variation with σ_{CTT}. There is an increase and divergence amongst the wavelengths at higher σ_{CTT}, although the error bars also get larger. The increases from the lowest to highest σ_{CTT} value are 25, 40 and 71 % in the $r_{e1.6}$, $r_{e2.1}$ $r_{e3.7}$ cases, respectively.

For the high θ_0 case, N_d values are higher than for low θ_0 for any given σ_{CTT} value as expected from the τ and r_e results and from the results of Sect. 3.2.3. As for at low θ_0, though, N_d is similar for the three wavelengths at low σ_{CTT} and there is little variation of N_d with σ_{CTT}. However, compared to at low θ_0, N_d from the different wavelengths diverge at a lower σ_{CTT} and at high σ_{CTT} they diverge more widely and produce much higher N_d values. Although, again, the error bars are large at high σ_{CTT} due to a lack of samples. The increases in N_d between the lowest σ_{CTT} value and σ_{CTT} = 2.6, where the maximum N_d occurs, are 19, 69, 117 % for the $r_{e1.6}$, $r_{e2.1}$ $r_{e3.7}$ cases, respectively. Thus at both low and high θ_0 the changes in N_d are smaller for $r_{e1.6}$.

It is interesting that at both low and high θ_0 there is little change in N_d with σ_{CTT} for low σ_{CTT}, as well as little diffence between N_d from the different wavelengths. The constant N_d is due to the cancellation of an increasing τ and increasing r_e as σ_{CTT} decreases. Since we might expect retrievals to be less prone to retrieval artifacts at low σ_{CTT}, the increase in τ with decreasing σ_{CTT} might suggest that the more homogeneous

ACPD
14, 303–375, 2014

clouds are actually physically thicker with a corresponding higher τ and higher r_e, and thus that the τ and r_e changes are physical rather than due to retrieval artifacts. Also, it is feasible that N_d might be the same for homogeneous and heterogeneous clouds if the aerosol supply was similar for both cases, which would be consistent with the above result. However, heterogeneity is also known to be associated with increased precipitation and thus an increased CCN sink and might also be associated with altered updraft speeds, which would alter N_d activation. Shedding further light on this is difficult, however, without further observations of the clouds in question.

3.5 Attribution of N_d changes with θ_0 to τ and r_e changes

It would be useful to be able to determine whether the changes in N_d that occur with increasing θ_0 were mainly due to changes in τ or changes in r_e. As shown already, the means of both quantities change with increasing θ_0 in the direction that causes an N_d increase, and so both are likely to contribute to some degree. Here we estimate the individual effects using a sensitivity analysis based upon Latin Hypercube Sampling for the change in N_d between the low and high θ_0 ranges that were used for the PDFs earlier. The details of this are described in Appendix D. Here we just discuss the main results, which are presented in Table 2. The main foci of the discussion here are the $\Delta N_{\Delta re}$ and $\Delta N_{\Delta\tau}$ values, which are the relative change in N_d between low and high θ_0 due to, respectively, changes in r_e only and changes in τ only (see Eq. D1).

When considering the whole cloud population, the results show that for the 1.6 µm band the contribution from changes in the τ distribution between low and high θ_0 have an effect on N_d that is roughly 5–6 times larger than that from r_e changes. This is perhaps not a surprise given the relative lack of change in r_e with θ_0 for that band. The r_e sensitivity is greater for the other bands; for the 2.1 µm band $\Delta N_{\Delta\tau}$ is a factor of two larger than $\Delta N_{\Delta r_e}$, whereas for the 3.7 µm band it is only 40 % larger. The greater sensitivity of N_d to τ biases between low and high θ_0 may be initially unexpected given the fact that the power to which r_e is raised to in Eq. (A1) is five times greater than that for τ.

ACPD
14, 303–375, 2014

For the high σ_{CTT} cases (i.e. for the more heterogeneous clouds), however, the balance between $\Delta N_{\Delta\tau}$ and $\Delta N_{\Delta r_e}$ shifts towards $\Delta N_{\Delta r_e}$. At low θ, $N_{\Delta\tau}$ is 2.5 times larger than $\Delta N_{\Delta r_e}$ for the 1.6 µm band. However, for the 2.1 and 3.7 µm bands the sensitivity to r_e is greater than the τ sensitivity; $\Delta N_{\Delta r_e}$ is 16 % larger than $\Delta N_{\Delta\tau}$ for 2.1 µm and 54 % larger for 3.7 µm.

Overall, these results suggest that biases in τ and r_e between low and high θ_0 can both be important causes of the increase in N_d at high θ_0, depending upon the r_e band and the cloud heterogeneity.

4 Discussion

4.1 Potential explanations for the r_e decrease with θ_0

In this section we discuss possible reasons for the decrease in r_e we observe as θ_0 increases. Table 3 summarizes three potential effects that could be a cause of r_e changes with θ_0 and the direction of their effects on r_e. These mechanisms are discussed in more detail below. It should be noted that there may be additional effects in operation that are not listed here. The three mechanisms are as follows:

1. The averaging scale r_e bias. There have been very few previous studies of the effect of θ_0 upon MODIS r_e retrievals. There have, however, been a few recent studies concerning the effects of cloud heterogeneity and 3-D radiative transfer on r_e retrievals, which may shed some light on the effect of high θ_0 on r_e retrievals. As discussed in Sect. 2.2.2, M06 and Z12 found opposite signs for the effect of sub-pixel averaging on r_e retrievals and it was suggested in Sect. 2.2.2 that a potential cause of the disagreement may be that the radiative transfer was performed at a higher θ_0 in M06 than in Z12. This indicates that varying θ_0 may influence the sign of r_e changes during sub-pixel averaging. However, in order to cause a negative r_e bias relative to the true r_e it would be required that there was a high degree of physical r_e variability within scale of the pixel. Z12 showed that

ACPD
14, 303–375, 2014

clouds physically tend to have more τ variability than r_e variability over the scale of a MODIS pixel and so an overall negative bias due to this effect seems unlikely. It is likely that in M06, rather than there being a high degree of physical r_e variability within the pixel scale, there was a high degree of R_{ab} variability caused by 3D radiative effects at high θ_0 due to the increased interception of photons by cloud sides and extra illumination and shadowing effects when the Sun is low in the sky (e.g. see Loeb et al., 1997). As explained in M06, this would have the effect of causing an overestimate of r_e at small averaging scales, with the positive bias reducing towards zero as the averaging scale is increased.

For the lower θ_0 results of Z12, increased averaging scales led to an increasingly positive r_e change. Therefore at sufficiently large averaging scales it is likely possible for r_e values at high θ_0 to be lower than those at low θ_0, as observed in our study. However, the relative changes of $r_{e2.1}$ and $r_{e3.7}$ give some indications that this averaging scale effect is unlikely to be the dominant cause of the r_e that we observed. This is discussed in the next section (Sect. 4.2).

2. The plane parallel (PP) r_e bias. As described in Sect. 2.2.1 non-absorbing reflectances (R_{nab}) from real heterogeneous clouds under 3-D radiative transfer and those from the PP model are found to change in opposite directions as θ_0 increases. This leads to an increasingly positive τ bias with increasing θ_0. If differences in absorbing wavelength reflectances (R_{ab}) between real and PP clouds varied in a similar manner with θ_0 then this would lead to a negative r_e bias (because r_e reduces with increasing R_{ab}) at high θ_0 and might provide another potential explanation for the observed result. Indeed Loeb and Coakley (1998) provide some evidence that R_{ab} may respond to 3-D radiative effects in a similar manner to R_{nab}.

3. The droplet size distribution (DSD) bias. Zhang (2013) found that wider DSDs than those assumed by the MODIS retrieval (MODIS assumes a single DSD width) would lead to a negative bias in the retrieved r_e.

ACPD
14, 303–375, 2014

In reality it is likely that combinations of all of these effects will occur to cause increases or decreases in r_e depending upon circumstances. Further work is needed to elucidate the signs and magnitudes of these effects under different viewing geometries, cloud fields, etc.

4.2 Potential explanations for why the r_e reduction with θ_0 varies amongst MODIS bands

Another interesting aspect of the current work is the stronger observed decrease of $r_{e3.7}$ with increasing θ_0 compared to $r_{e2.1}$, along with the lack of change of $r_{e1.6}$. Here we discuss possible reasons for this by considering the likely relative magnitudes of the three effects mentioned in the previous subsection for the different MODIS bands (see Table 3). We attempt to estimate these relative changes for effect (1), although these estimates are fairly uncertain. For effect (2) there has been little previous work on this and such work is beyond the scope of this study and so we leave this as an unknown. Also, most previous work has only considered differences between $r_{e2.1}$ and $r_{e3.7}$.

As mentioned in the previous subsection, it seems likely that in the model results of M06 3D effects at high θ_0 caused a positive bias in r_e when the averaging scale was small (effect 1 above and in Table 3). Interestingly, such an overestimate is likely to be larger for $r_{e3.7}$ than for $r_{e2.1}$. Figure 14 shows an example of why this is so. The assumption is made that there are a number of small regions of cloud with the same r_e (= 14 µm) and τ (= 21.4). These correspond to R_{ab} and R_{nab} values that can be determined using PP LUTs similar to those used operationally for MODIS retrievals. It is then assumed that 3D radiative transfer at high θ_0 causes the absorbing and non-absorbing reflectances of half of these regions to be decreased and half to be increased by the same amount, ΔR=0.05, from the PP values. If PP retrievals are then performed upon these distorted reflectances then the retrieved r_e increases relative to the true r_e. However, the retrieved $r_{e3.7}$ is 4 µm larger than $r_{e2.1}$ ($r_{e2.1}$ = 15.3 µm, $r_{e3.7}$ = 19.3 µm). $r_{e1.6}$ = 14.7 µm and so experiences the least bias.

ACPD
14, 303–375, 2014

Table 4 shows the magnitude of this effect at different θ and ϕ and reveals that the bias from the true values and the difference between $r_{e3.7}$ and $r_{e2.1}$ is likely to be lower at high θ (50°) than at nadir. The biases when $\phi = 30°$ are especially low, suggesting that 3-D effects are highly sensitive to the viewing geometry. The sign of the relative differences between the different bands is maintained at all the viewing geometries, with $r_{e3.7} > r_{e2.1} > r_{e1.6}$.

Thus for high resolution retrievals at high θ_0 3D effects are likely to cause on over-estimate in r_e. Then upon averaging reflectances over ever larger averaging scales the retrieved r_e would be expected to decrease towards the true value as the positive and negative reflectance changes start to cancel out. The above example suggests that for high θ_0, at any given averaging scale we would expect $r_{e3.7}$ to be larger than $r_{e2.1}$. However, this was not what was observed, which would indicate that 3-D effects of this type are not the sole cause of the observed retrieved r_e values. Some caveats here are that for real-world 3D effects it may not be the case that ΔR values are the same for all of the non-absorbing bands and it may not be the case that positive ΔR values are the same as negative ones. The latter would mean that the overall reflectance change was zero on average, which according to the works cited in Sect. 2.2.1 (regarding the PP r_e bias) is not likely to be the case. In addition, the other effects mentioned (the PP r_e bias and the DSD bias) also have the potential to interact with these effects to produce the result observed in this paper. For example, Zhang (2013) showed that the decrease in r_e due to the effects of a wide DSD are likely to be greater for $r_{e3.7}$ than for $r_{e2.1}$, which is consistent with the results presented here for high θ_0. However, it is unclear why this would not also be observed at low θ_0. Further work is required to investigate these matters, which is beyond the scope of this study.

4.3 Discussion on the observed changes in the retrieval of r_e with cloud heterogeneity

The results described in Sect. 3.4.2 and discussed in Sect. 4.2 showed that a general decrease in $r_{e2.1}$ and $r_{e3.7}$ occurs with increasing σ_{CTT} for all the θ_0 values studied here

ACPD
14, 303–375, 2014

($\theta_0 > 50^\circ$), but that there was little change in $r_{e1.6}$. $r_{e3.7}$ was also found to decrease at a faster rate than $r_{e2.1}$. Both θ_0 increases and physical cloud top heterogeneity (as described by σ_{CTT}) are likely to cause increases in reflectance heterogeneity. This is consistent with the observed greater decrease in $r_{e3.7}$ compared to $r_{e2.1}$ as σ_{CTT} increases and the results from Sect. 3.2.2 whereby $r_{e3.7}$ was the wavelength most strongly affected by θ_0 changes. However, a significant caveat is that it is not clear that σ_{CTT} is a good indicator of sub-pixel heterogeneity. Since the cloud top temperature is retrieved at 5 km resolution σ_{CTT} might not correlate with variability at scales smaller than this.

Another complicating factor here is that there may be some physical cloud changes that occur as a function of σ_{CTT} as was also indicated by the variation in τ with σ_{CTT}. This could alter the vertical structure of droplet radius and thus the relative r_e values from the different bands. At low θ_0 the clouds with more homogeneous cloud tops had $r_{e3.7} > r_{e2.1} > r_{e1.6}$, which is actually what might be expected from a cloud in which r_e increased with height due to the increased penetration depth of the smaller wavelengths of light (e.g. see Platnick, 2000). Many studies have suggested that the differences between MODIS $r_{e1.6}$, $r_{e2.1}$ and $r_{e3.7}$ can impart information on the vertical structure of r_e near cloud top (Chang and Li, 2002, 2003; Chen et al., 2007; Seethala and Horvath, 2010; Nakajima et al., 2010a, b). It would be expected that r_e would increase monotonically with height in an idealised cloud with no entrainment occurring and no drizzle drops present. In reality both may occur and so may have the potential to reverse this gradient. The observation from Fig. 12a that the $r_{e1.6}$, $r_{e2.1}$ and $r_{e3.7}$ values are consistent with such a gradient reversal between low and high σ_{CTT} is interesting since high σ_{CTT} values are likely to be associated with more prevalent drizzle.

However, the work of Z12 and Zinner et al. (2010) suggests that precipitation is unlikely to have a large impact on r_e retrievals. In addition, theoretical work presented in King and Vaughan (2012) indicates that measurement and plane parallel modelling uncertainties are likely to be too large to accurately discern differences in the vertical variation of r_e using the MODIS bands available.

ACPD
14, 303–375, 2014

Despite the uncertainties in determining the relative importance of physical and retrieval artifacts as a function of σ_{CTT} in our results, it can be said that θ_0 affects the relative values of $r_{e1.6}$, $r_{e2.1}$ and $r_{e3.7}$ at all σ_{CTT}, and therefore that θ_0 effects will need to be considered if attempting to determine vertical variation information from MODIS observations.

5 Summary and implications

In this paper we have examined the effect of Solar Zenith Angle (θ_0) on MODIS retrievals of τ, r_e and N_d, where the latter is a function of the two former quantities (Eq. A1). To do this we examined Arctic stratocumulus clouds in a region of the Norwegian/Barents Sea (72 to 75° N, −3 to 48° E). This region has the advantage of being completely free of sea-ice throughout the year, but yet it is far enough north to experience several Terra and Aqua overpasses per day. This means that θ_0 retrieval effects can be examined in actual MODIS data by utilizing the diurnal cycle. Potential latitudinal and seasonal variations of cloud properties can be avoided by focusing upon a short time period (13–30 June) and upon a small latitude range. However, there is the possibility that there are physical changes of the clouds during the diurnal cycle. We argue that these changes are likely to be small because the diurnal cycle here is one of the weakest on Earth in terms of LWP variation (O'Dell et al., 2008), probably because the Sun is only below the horizon for a short period in this mid-summer period. We have also showed that the variation within our region of retrieved N_d with local time is more characteristic of a θ_0 retrieval artifact than of a diurnal cycle.

In addition to this, we have looked for differences between low and high θ_0 periods in quantities that give some information on the physical states of the clouds, but that are not affected by the types of optical retrieval bias that we are searching for. These include the MODIS cloud top temperature (CTT) and the variability of MODIS CTT (σ_{CTT}). CTT and σ_{CTT} PDFs are virtually identical for the low and high θ_0 ranges, sug-

ACPD
14, 303–375, 2014

gesting that there is little physical difference in the cloud populations at these different times of day in terms of cloud thickness and heterogeneity.

The results of the θ_0 analysis showed that the mean τ was fairly constant between $\theta_0 = 50^\circ$ and $\sim 65^\circ$, but then increased rapidly with an increase of over 70 % between the lowest and highest θ_0. In contrast the change between the low and high Sensor Zenith Angles (θ) ranges was small at both low and high θ_0. The change due to θ_0 is consistent with previous studies on the effect of θ_0 on τ (Loeb and Davies, 1996, 1997; Loeb and Coakley, 1998; Loeb et al., 1998, 1997; Varnai and Davies, 1999). From these studies it was ascertained that the bias arose through differences in the how the reflectance of real (heteorogeneous) clouds changed with θ_0 relative to the plane parallel clouds used to model the reflectance-τ relationships used for retrievals. These studies suggested that the difference was mainly a result of variability in cloud top height rather than extinction variability. The lack of θ sensitivity is perhaps more surprising, although studies have shown that the magnitude and sign of the effect of changing θ is dependent upon whether back or forward scatter viewing angles are being employed and on the cloud thickness (Loeb and Davies, 1997; Loeb and Coakley, 1998; Loeb et al., 1998; Liang and Girolamo, 2013). The relative azimuth angles (ϕ) of the retrievals in this study were all side scatter viewing angles.

r_e values retrieved using the 2.1 and 3.7 µm bands ($r_{e2.1}$ and $r_{e3.7}$, respectively) were found to decrease with θ_0, with effects starting at around $\theta_0 = 65^\circ$, which is consistent with the θ_0 at which the τ increases occurred. At low θ_0 the r_e values from the three different MODIS bands agree to within around 0.2 µm, whereas at high θ_0 the spread is closer to 1 µm. The percentage changes of r_e with θ_0 were somewhat lower than those for τ being around 5 % and 7 % for $r_{e2.1}$ and $r_{e3.7}$, respectively. However, for $r_{e1.6}$ there was very little change with θ_0. Larger decreases in r_e, which depended upon the MODIS r_e band, were observed as the cloud top heterogeneity changed from low to high values; decreases of 25–30 % for $r_{e3.7}$, $\sim$ 20 % for $r_{e2.1}$ and 10 % for $r_{e1.6}$. However, it is possible that the clouds were changing physically with cloud top heterogeneity and that such changes may affect the retreived r_e as well. Also, the measure

ACPD
14, 303–375, 2014

of cloud top heterogeneity used is only capable of quantifying heterogeneity at scales resolved by the 5 km data resolution. Higher resolution measures of heterogeneity may be preferable for this type of work unless lower resolution variability correlates with high resolution variability.

Whilst the r_e changes are quite small they are not insignificant for the calculation of N_d, since the equation relating N_d to τ and r_e implies a sensitivity to r_e changes that is five times greater than the sensitivity to τ changes. Using Latin Hypercube Sampling (LHS) sensitivity analysis we assessed the relative contributions of the τ increase and r_e decrease to the N_d changes between low and high θ_0. The overall N_d increase between low and high θ_0 varied between ~ 40 and 70 % depending on MODIS band and θ. When considering the studied cloud population as a whole, it was found that the N_d contribution from the τ biases and r_e biases were roughly comparable for $r_{e3.7}$. However, for the other r_e bands the τ changes were considerably more important (roughly twice the contribution for $r_{e2.1}$ and six times for $r_{e1.6}$). However, when considering only the more heterogeneous clouds, the importance of the r_e biases was considerably enhanced for both $r_{e2.1}$ and $r_{e3.7}$; τ and r_e bias contributions were comparable for $r_{e2.1}$ and for $r_{e3.7}$ bias contributions from r_e were ~ 50 % greater.

5.1 Implications for Level-3 retrievals and a new dataset

The analysis presented in this paper suggests that when θ_0 is larger than around 65°, MODIS retrievals of τ, r_e and N_d become unreliable due to optical artifacts. This suggest that such retrievals should not be used, which unfortunately would mean that large regions of the globe at higher latitudes would need to be excluded in their winter seasons when the Sun is low in the sky. The problem is exacerbated for the MODIS daily L3 product since this produces averages of τ and r_e over all overpasses that occur on a given day for which $\theta_0 < 81.4°$. Some locations will experience several overpasses per day and thus retrievals will be made at a range of θ_0 values. At some locations on a given day some of the daily overpasses will occur at θ_0 near 65° and therefore might not be affected by the biases seen here too greatly, but other overpasses will occur

ACPD
14, 303–375, 2014

at much greater θ_0. For these locations some "good" data is available, but for the L3 product it will be averaged in with "bad" data. Thus, taking the conservative approach it would be prudent to discard the daily averaged L3 value. This problem is more likely to occur as the number of daily overpasses increases, which is generally the case moving poleward. Analysis suggests that the most strongly affected regions/times for which both good and bad data will be contained in L3 will be those poleward of $\sim \pm 64^\circ$ for the spring and summer seasons. At higher latitudes and in the winter season there will still be L3 data for which $\theta_0 > 65^\circ$, but in those cases there will be no good data that is also salvageable. Overpasses with $\theta_0 > 65^\circ$ can occur at latitudes as low as $\sim 28^\circ$ in mid-winter and thus the θ_0 bias problem has the potential to affect very large regions of the globe. Given this, an operational solution to the problem would ideally be sought.

We have compiled our own version of the Level-3 product using similar procedures to those used for the operational product, but excluding data from overpasses $> 65^\circ$. In a follow-on paper we will examine this dataset in order to identify the main problem regions/times and we will also explore science problems relating to N_d, but in the light of the θ_0 biases identified here.

Appendix A

The method used to estimate droplet concentration

The formula for the estimation of N_d from τ and r_e as derived in Boers et al. (2006) and B07 is:

$$N_d = \frac{2\sqrt{10}}{k\pi Q^3}\left(\frac{c(T,P)\tau}{\rho_w r_e^5}\right)^{1/2} \quad \text{(A1)}$$

$$k = (r_v/r_e)^3,$$

ACPD
14, 303–375, 2014

where τ is the cloud optical thickness, r_e and r_v are the cloud top effective and volume mean radius, respectively, k is cube of the ratio of r_v to r_e, ρ_w is the density of water and Q is the scattering efficiency. Q has been shown to have a constant value very close to 2 for droplet radii that are much larger than the wavelength of light concerned (B07). c is the rate of increase of liquid water content (q_L) with height (dq_L/dz, with units kgm^{-4}) and is referred to as the "condensation rate" in B07, or the "water content lapse rate" in Painemal and Zuidema (2011, hereafter PZ11). Albrecht et al. (1990) and Ahmad et al. (2013) give two alternative derivations of this quantity. c depends more strongly on the temperature (T) than on the pressure (P). For example, the percentage change due to a pressure decrease from 850 to 650 hPa are 15.5, 12.0 and 8.1 % at temperatures of 283, 273 and 263 K, respectively. Thus the pressure dependence is greater at warmer temperatures. The change as the temperature decreases from 283 to 263 K is 47.8 and 43.2 % at 850 and 650 hPa, respectively. Since N_d calculations are generally applied to low clouds only, the range of pressure of the studied clouds is likely to be smaller than that of temperature, although pressure dependence may be important for the warmest clouds. Hence, we use a constant P value of 850 hPa due to likely inaccuracies when determining P from MODIS.

Although c and T should strictly be taken to vary with height, in this manuscript we use the MODIS CTT to calculate a constant c value for each datapoint for use in Eq. (A1). Since for most clouds the change in T throughout their depth is fairly small and given the relatively weak dependence of c on T, this makes a negligible difference. For example, using a height dependent c, numerical calculations show that an adiabatic cloud with $\tau = 80$, $r_e = 21$ µm, a cloud base pressure of 900 hPa and a cloud base temperature of 283 K, would be 976 m thick with $N_d = 60.2\,cm^{-3}$ after making the assumption that N_d is constant with height. Approximating c as a constant, calculated from the cloud top temperature and a pressure of 850 hPa (the constant value assumed in the calculations in this manuscript), results in an underprediction of N_d of only 2 %. Since this example represents a very thick cloud, the error in most circumstances is likely to be smaller than this.

ACPD
14, 303–375, 2014

This derivation of N_d requires a number of assumptions to be made about the sampled clouds. The first assumption is that N_d is constant with height throughout the cloud depth. However, there is good observational evidence that this is the case for a number of different types of clouds in a variety of different regions, but in particular for warm stratiform clouds (PZ11; Miles et al., 2000; Wood, 2005a).

Another assumption is that the clouds are adiabatic, or some constant fraction of adiabatic. For all but the deepest of clouds this equates to q_L increasing linearly with height. There have been in-situ and surface remote sensing observational studies that indicate that this assumption is accurate (Albrecht et al., 1990; Zuidema et al., 2005). From aircraft observations made in the SE Pacific region PZ11 found linear q_L profiles within stratocumulus that on average had c values that were 70 % of adiabatic, i.e.

$$c_{\text{observed}} = f c_{\text{adiabatic}}, \tag{A2}$$

with $f = 0.7$ being the sub-adiabaticity. This is approximately consistent with Wood (2005b), which shows f values of 0.6–0.9 for single layer stratocumulus. It is possible that this sub-adiabaticity fraction varies depending upon region; cloud type and depth; and upon conditions, e.g. whether the cloud is precipitating, whether ice is present, the degree of entrainment, etc. However, as can be seen from Eq. (A1) the dependence of N_d on c is fairly weak, being proportional only to $c^{0.5}$.

A further assumption for which there is also good evidence is that k assumes a fairly constant value. Martin et al. (1994) found a k range of 0.7–0.8. PZ11 found profile averaged k values of around 0.8, but an increase to 0.88 near cloud top. However, here we adopt the value of $k = 0.8$, which was used in B07 and as the "baseline" case in PZ11.

In line with other studies, PZ11 found that, on average, MODIS r_e values were 15–20 % too large compared to the in-situ observations. Potential reasons for this discrepancy are discussed in Sect. 4. However, PZ11 showed that when the modified f and k values mentioned above (= 0.8 and 0.88, respectively) were applied in Eq. (A1), along with a constant correction factor that reduced r_e by 15 %, the resulting N_d values were

ACPD
14, 303–375, 2014

only 6 % smaller than that using the standard MODIS r_e and the more conventional values of the k and f parameters (0.8 and 1, respectively). This was because the f and k modifications mostly canceled out the r_e modifications. In the present study we leave these factors unchanged from the "conventional" values, but note that the N_d values will be similar to those that would be produced if the adjusted parameters that were suggested in PZ11 were applied. The same would not be true for other derived quantities such as LWP and cloud thickness (see B07).

Appendix B

Discussion on the effect of the diurnal cycle on our results

Observations show that subtropical stratocumulus clouds tend to thicken at nighttime due to the absence of shortwave heating at cloud top (Wood, 2012) and that this is accompanied by increased drizzle rates. Such clouds generally reach their thickest in the early morning, just before the sun comes up. Thus, for those clouds we might expect τ to be highest at this time due to enhanced LWP. N_d effects might also influence τ, although for adiabatic clouds (see Appendix A) $\tau \propto N_d^{1/3}\mathrm{LWP}^{5/6}$ and thus more sensitivity to LWP might be expected. However, r_e is more sensitive to N_d changes than LWP changes since $r_e \propto N_d^{-1/3}\mathrm{LWP}^{1/6}$. There are no measurements of the diurnal cycle of N_d in stratocumulus known to the authors. The N_d diurnal cycle is likely to be complicated due to competing (but relatively weak) sources and sinks of N_d at nighttime; enhanced updrafts and surface fluxes may lead to an additional N_d source, whereas enhanced precipitation is likely to cause N_d depletion. However, we note that the timescales that govern boundary layer sources and sinks of CCN are of the order of a few days (Wood, 2006; Wood et al., 2012) such that any change in these processes due to θ_0 variation is likely to have a damped effect upon CCN concentrations and thus

ACPD
14, 303–375, 2014

likely upon N_d. The additional LWP at nighttime in stratocumulus would likely lead to an increase in r_e in the absence of N_d changes.

However, the clouds in our study region may behave differently than those in other stratocumulus regions. In summer, at the high latitudes of our study area, the difference in θ_0 between midday and 12 h later is much less than at lower latitudes and this is likely to reduce the amplitude of the diurnal cycles of cloud properties such as LWP, τ, r_e and N_d. Measurements of the diurnal cycles of τ, r_e and N_d are lacking for the clouds in the region of our study. However, O'Dell et al. (2008) reported that LWP diurnal amplitudes in the area were $<\sim$ 10–20 % in July (June results were not shown), which is amongst the lowest value found globally. Other stratocumulus regions show amplitudes of 30–50 % (see also Wood et al., 2002). The local time of maximum LWP was around 03:00–06:00 LT, which is a little earlier than for other stratocumulus regions where 06:00–09:00 LT was more typical. These times are consistent with the time at which the local θ_0 decreases to below around 70–80° suggesting that at this θ_0 shortwave heating effects start to reduce LWP due to solar heating as the sun rises. A 10–20 % increase in LWP corresponds to an approximate increase in τ of 8–17 % and an r_e increase of $\sim$ 1.5–3 %, if it is assumed that N_d stays constant. This issue, with reference to our results, is discussed in Sect. 3.3.

Observations of the diurnal cycles of Arctic clouds have been made (Shupe, 2011; Tjernstrom, 2007). Shupe (2011) showed observations of the diurnal cycle of cloud fraction, which revealed a very weak amplitude cycle. The largest amplitudes were found for mixed-phase clouds during times of the year when the Sun was both above and below the horizon during a day. Even then the diurnal range was only 8 %; for liquid clouds the range was generally less than 4 %. Tjernstrom (2007) showed that the diurnal cycle of Arctic stratocumulus cloud thickness was almost the opposite of that seen at lower latitudes with the thickest clouds occurring between approximately 09:00 and 16:00 LT. However, the diurnal amplitude of θ_0 at the time of that study was very small ($\sim$ 2–5°) and thus there would be very little variability in solar cloud top heating

ACPD
14, 303–375, 2014

(unless there were other diurnally dependent effects, e.g. changing cloud cover above the stratocumulus).

Another problem is that the above mentioned Arctic observations were all either made at much higher latitudes than our observation region, or they have were made over ice covered surfaces (land or sea-ice). Thus it is doubtful whether they are representative of our region, especially since our region shows some qualitative similarity to subtropical stratocumulus, at least in terms of the LWP diurnal cycle.

Appendix C

Discussion on the likelihood of ice formation in the sampled cloud population

For clouds with temperatures throughout that are warmer than −5 °C, de Boer et al. (2011) showed that liquid-only clouds accounted for approximately 22, 65 and 90 % of clouds observed at three Arctic locations and very little ice-only cloud was observed. Whilst those locations were not near those of our study, and were not open ocean regions they likely provide some insight into the issue. As the temperature increased, the dominance of liquid-only cloud became more complete. The preponderance of mixed phase and liquid-only cloud at temperatures > −5 °C is also supported by the observed (at various locations worldwide) very low concentrations of ice nulcei (IN) with which to initiate primary ice formation (DeMott et al., 2010) at such relatively warm temperatures.

However, the Hallett Mossop secondary ice multiplication mechanism is known to operate between the temperatures of −3 and −8 °C (Hallett and Mossop, 1974), with maximum multiplication occurring in the middle of this temperature range. Seeding of such relatively warm clouds by falling ice from clouds above, followed by Hallet Mossop ice production is thought to be a cause of significant ice production even in Antarctic stratus clouds (Grosvenor et al., 2012) where aerosol concentrations are very low. Nevertheless, Grosvenor et al. (2012) also showed that the Hallett Mossop process does

ACPD
14, 303–375, 2014

not always operate in all supercooled cloud, even if it is within the right temperature range, likely because it also depends on the droplet size distribution (Mossop, 1985; Saunders and Hosseini, 2001) and because ice seeding may not always occur even with high cloud above, e.g. due to a lack of ice precipitation from the high cloud, intervening dry layers, etc. A further complication is that some evidence suggests that it is the temperature at the surface of the riming ice particle that governs the process rather than the ambient air temperature (Heymsfield and Mossop, 1984). The ice surface temperature can be warmer than the air temperature due to latent heat release from the freezing liquid. This would reduce the likelihood of the Hallett Mossop process at the warmer temperature part of the −3 to −8 °C temperature range.

Appendix D

Sensitivity analysis of N_d changes with θ_0 using latin hypercube sampling

Here we describe in detail the method used to explore the relative importance of τ and r_e changes in causing the increase in N_d between low and high θ_0. Latin Hypercube Sampling (LHS) sampling was used, which allows us to include the effects of the data spread and distribution shapes on the sensitivity analysis. Using LHS we constructed pairs of τ and r_e values, each containing 100 000 datapoints, which retained the same distribution shapes as the τ and r_e PDFs shown in Figs. 7 and 8. This is done for both the low and high θ_0 ranges and for combinations of the two. It is also possible to introduce correlation between τ and r_e using the method of Iman and Conover (1982).

Using the reconstructed sample sets we calculate N_d values using Eq. (A1). The accuracy of the reconstructed samples is demonstrated in Table A1, which shows the quantity s_{lhs}. This is the ratio of the mean N_d as calculated from the LHS sets and the actual N_d value from the real data. The values are all fairly close to one, which gives confidence in the use of these samples in the sensitivity analysis. However, all of the values except for one are ≥ 1 suggesting a tendency for an overestimate. The largest

ACPD
14, 303–375, 2014

overestimates (s_{lhs} = 1.09) coincide with the highest positive correlations between τ and r_e and the lowest with the most negative correlations, suggesting that the combination of low r_e and high τ, and vice versa, leads to the largest overall N_d values through the non-linearity of Eq. (A1). When the observed correlations (see Table 1) are included in the LHS sampling, the s_{lhs} values are brought closer one; s_{lhs} then ranges between 1.0 and 1.03 (not shown).

With the knowledge that the constructed LHS set of (τ,r_e) pairs approximate the N_d values produced using the actual τ and r_e values, we can now use them for the sensitivity analysis with more confidence. We proceed by combining the low θ_0 LHS set for τ with the high θ_0 set for r_e in order to calculate a mean N_d, denoted as $N_{\Delta re}$. $\Delta N_{\Delta re}$, which is listed in Table 2 is thus the relative change in N_d between low and high θ_0 due to changes in r_e only:

$$\Delta N_{\Delta re} = 100(N_{\Delta re} - N_{low})/N_{low}, \quad \text{(D1)}$$

where N_{low} is the N_d value at low θ_0. In a similar way we calculated $\Delta N_{\Delta\tau}$ using the r_e set for low θ_0 and the τ set for high θ_0. These vlaues are discussed in Sect. 3.5.

As mentioned above, incorporating the correlation between τ and r_e brought the LHS N_d values closer to the actual values for the low and high θ_0 sets. However, it is difficult to choose values for the correlation between the τ LHS set at low θ_0 and the r_e set at high θ_0 (and vice versa) since the correlations between τ and r_e were seen to vary with θ_0 (Table 1). Thus, we use zero correlation here, but note that the error introduced is likely to be less than 10 %.

As an aside, it is interesting to note that N_d values calculated using the mean τ and r_e values of the distributions (using Eq. A1) produce lower values than the actual N_d values. This is probably due to the high degree of non-linearity in the N_d equation so that combinations of low r_e and high τ from values in the tails of the distributions lead to very large N_d values. We define w as the ratio of the actual N_d values to those

ACPD
14, 303–375, 2014

calculated using the mean values:

$$w = \frac{\overline{C}\,\overline{\tau^{0.5}}\,\overline{r_e^{-2.5}}}{\overline{C}\,\overline{\tau^{0.5}}\,\overline{r_e^{-2.5}}} \qquad \text{(D2)}$$

$$C = \frac{2\sqrt{10}}{k\pi Q^3}\left(\frac{c(T,P)}{\rho_w}\right)^{0.5}$$

Values of w for the different datasets are listed in Table A1 and range from 1.07 to 1.15, with most values being around 1.09–1.10. The highest values occur for the 3.7 µm band. Thus, care must be taken when using the mean τ and r_e of a set of values to calculate the mean N_d of that set. This could also have implications for the method used here whereby we use the mean τ and r_e values over a $1^\circ \times 1^\circ$ area. However, it seems likely that if τ and r_e values from very small regions (e.g. single MODIS pixels) are used then the calculated N_d might also become prone to biases due to uncertainties, heterogeneities, etc, which may become "smoothed out" by averaging over larger regions. Thus, it seems likely that there is an optimal averaging scale for τ and r_e for the calculation of N_d.

The fact that the w values are fairly constant across all of the different datasets in Table A1 suggests that, whilst using mean values may not give the correct absolute values of N_d, it may be possible to use them for a sensitivity analysis in order to calculate $\Delta N_{\Delta\tau}$ and $\Delta N_{\Delta re}$. If N_d calculated using the mean is wrong by the same factor at low and high θ_0 it seems likely that the sensitivity test values $N_{\Delta\tau}$ and $N_{\Delta re}$ would be wrong by the same factor. In that case the associated relative increases in N_d from low θ_0 values (as in Eq. D1) will be the same as for the LHS sensitivity analysis (with the assumption that the LHS method is completely accurate). Table 2 lists the ratios between $\Delta N_{\Delta\tau}$ and $\Delta N_{\Delta re}$ calculated from the mean values to those calculated using

ACPD
14, 303–375, 2014

the LHS:

$$t_{\Delta\tau} = \frac{\Delta N_{\Delta\tau,\mathrm{mean}}}{\Delta N_{\Delta\tau,\mathrm{lhs}}}$$
$$t_{\Delta\mathrm{re}} = \frac{\Delta N_{\Delta\mathrm{re},\mathrm{mean}}}{\Delta N_{\Delta\mathrm{re},\mathrm{lhs}}} \quad \text{(D3)}$$

Here the ΔN_d values are relative changes as in Eq. (D1). The results show that $\Delta N_{\Delta\tau}$ and $\Delta N_{\Delta\mathrm{re}}$ are within 16 % of the LHS values for the 2.1 and 3.7 µm bands and often very close to one. The errors in $\Delta N_{\Delta\mathrm{re}}$ are larger than this for two of the cases for the 1.6 µm band, which is likely because the $\Delta N_{\Delta\mathrm{re}}$ values are so small. Errors for $\Delta N_{\Delta\mathrm{re}}$ are generally larger than for $\Delta N_{\Delta\tau}$ even when the magnitude of the $\Delta N_{\Delta\tau}$ and $\Delta N_{\Delta\mathrm{re}}$ values are similar. Overall, the results suggest that LHS analysis is perhaps not required for N_d sensitivity calculations since using mean values produces generally similar results. However, if the spread or shapes of the τ and r_e distributions between low and high θ_0 were very different then this may not be the case since the w values would then be likely to also change with θ_0. Additionally, significant variations in the correlation between τ and r_e distributions at low and high θ_0 would likely lead to decreased accuracy in the sensitivity analysis for both the LHS method and that using the mean values.

Acknowledgements. The authors would like to thank Zhibo Zhang and Dan Miller for the LUTs used in this paper, as well as Marc Michelsen for extensive technical support. We acknowledge the World Climate Research Programme's Working Group on Coupled Modelling, which is responsible for CMIP, as well as IPSL for making the CALIPSO data used in this study available. For CMIP the US Department of Energy's Program for Climate Model Diagnosis and Intercomparison provides coordinating support and led development of software infrastructure in partnership with the Global Organization for Earth System Science Portals. MODIS data were obtained from the NASA Goddard Land Processes data archive. The sea-ice data was provided by the NSDIC.

ACPD
14, 303–375, 2014

References

Ahmad, I., Mielonen, T., Portin, H. J., Arola, A., Grosvenor, D. P., Mikkonen, S., Leskinen, A., Komppula, M., Lehtinen, K. E. J., Laaksonen, A., and Romakkaniemi, S.: Long term measurements of cloud droplet concentrations and aerosol-cloud interactions in boreal boundary layer clouds, Tellus B, 65, 20138, doi:10.3402/tellusb.v65i0.20138, 2013. 340

Albrecht, B., Fairall, C., Thomson, D., White, A., Snider, J., and Schubert, W.: Surface-based remote-sensing of the observed and the adiabatic liquid water-content of stratocumulus clouds, Geophys. Res. Lett., 17, 89–92, doi:10.1029/Gl017i001p00089, 1990. 340, 341

Bennartz, R.: Global assessment of marine boundary layer cloud droplet number concentration from satellite, J. Geophys. Res.-Atmos, 112, D02201, doi:10.1029/2006JD007547, 2007. 306

Boers, R., Acarreta, J. R., and Gras, J. L.: Satellite monitoring of the first indirect aerosol effect: retrieval of the droplet concentration of water clouds, J. Geophys. Res.-Atmos., 111, D22208, doi:10.1029/2005jd006838, 2006. 306, 307, 339

Cahalan, R., Ridgway, W., Wiscombe, W., Bell, T., and Snider, J.: The albedo of fractal stratocumulus clouds, J. Atmos. Sci., 51, 2434–2455, doi:10.1175/1520-0469(1994)051<2434:TAOFSC>2.0.Co;2, 1994. 309, 315

Chang, F.-L. and Li, Z.: Estimating the vertical variation of cloud droplet effective radius using multispectral near-infrared satellite measurements, J. Geophys. Res.-Atmos., 107, AAC 7-1–AAC 7-12, doi:10.1029/2001JD000766, 2002. 335

Chang, F.-L. and Li, Z.: Retrieving vertical profiles of water-cloud droplet effective radius: algorithm modification and preliminary application, J. Geophys. Res., 108, 4763, doi:10.1029/2003JD003906, 2003. 335

Chen, R., Chang, F.-L., Li, Z., Ferraro, R., and Weng, F.: Impact of the vertical variation of cloud droplet size on the estimation of cloud liquid water path and rain detection, J. Atmos. Sci., 64, 3843–3853, doi:10.1175/2007JAS2126.1, 2007. 335

Chepfer, H., Bony, S., Winker, D., Cesana, G., Dufresne, J. L., Minnis, P., Stubenrauch, C. J., and Zeng, S.: The GCM-oriented CALIPSO cloud product (CALIPSO-GOCCP), J. Geophys. Res.-Atmos., 115, D00H16, doi:10.1029/2009JD012251, 2010. 320

Davies, R.: Effect of finite geometry on 3-dimensional transfer of solar irradiance in clouds, J. Atmos. Sci., 35, 1712–1725, doi:10.1175/1520-0469(1978)035<1712:TEOFGO>2.0.CO;2, 1978. 309

ACPD
14, 303–375, 2014

de Boer, G., Morrison, H., Shupe, M. D., and Hildner, R.: Evidence of liquid dependent ice nucleation in high-latitude stratiform clouds from surface remote sensors, Geophys. Res. Lett., 38, L01803, doi:10.1029/2010GL046016, 2011. 320, 344

DeMott, P. J., Prenni, A. J., Liu, X., Kreidenweis, S. M., Petters, M. D., Twohy, C. H., Richardson, M. S., Eidhammer, T., and Rogers, D. C.: Predicting global atmospheric ice nuclei distributions and their impacts on climate, P. Natl. Acad. Sci. USA, 107, 11217–11222, doi:10.1073/pnas.0910818107, 2010. 320, 344

Foot, J.: Some observations of the optical-properties of clouds.1. Stratocumulus, Q. J. Roy. Meteor. Soc., 114, 129–144, doi:10.1256/Smsqj.47906, 1988. 305

Grosvenor, D. P., Choularton, T. W., Lachlan-Cope, T., Gallagher, M. W., Crosier, J., Bower, K. N., Ladkin, R. S., and Dorsey, J. R.: In-situ aircraft observations of ice concentrations within clouds over the Antarctic Peninsula and Larsen Ice Shelf, Atmos. Chem. Phys., 12, 11275–11294, doi:10.5194/acp-12-11275-2012, 2012. 344

Hallett, J. and Mossop, S.: Production of secondary ice particles during the riming process, Nature, 249, 26–28, doi:10.1038/249026a0, 1974. 344

Heymsfield, A. J. and Mossop, S. C.: Temperature dependence of secondary ice crystal production during soft hail growth by riming, Q. J. Roy. Meteor. Soc., 110, 765–770, doi:10.1002/qj.49711046512, 1984. 345

Hoose, C., Kristjánsson, J. E., Iversen, T., Kirkevåg, A., Seland, Ø., and Gettelman, A.: Constraining cloud droplet number concentration in GCMs suppresses the aerosol indirect effect, Geophys. Res. Lett., 36, L12807, doi:10.1029/2009GL038568, 2009. 306, 307

Iman, R. and Conover, W.: A distribution-free approach to inducing rank correlation among input variables, Commun. Stat. B-Simul., 11, 311–334, doi:10.1080/03610918208812265, 1982. 345

IPCC: Climate Change 2007 – The Physical Science Basis: Working Group I Contribution to the Fourth Assessment Report of the IPCC, Cambridge University Press, Cambridge, UK, New York, NY, USA, 2007. 306

King, M. D., Tsay, S.-C., Platnick, S. E., Wang, M., and Liou, K. N.: Cloud retrieval algorithms for MODIS, Optical thickness, effective particle radius, and thermodynamic phase, NASA, MODIS Algorithm Theoretical Basis document No. ATBD-MOD-05, 1997. 305, 318

King, M. D., Platnick, S., Yang, P., Arnold, G., Gray, M., Riedi, J., Ackerman, S., and Liou, K.: Remote sensing of liquid water and ice cloud optical thickness and effective radius in the

ACPD
14, 303–375, 2014

Arctic: application of airborne multispectral MAS data, J. Atmos. Ocean. Tech., 21, 857–875, doi:10.1175/1520-0426(2004)021<0857:RSOLWA>2.0.CO;2, 2004. 317
King, N. J. and Vaughan, G.: Using passive remote sensing to retrieve the vertical variation of cloud droplet size in marine stratocumulus: an assessment of information content and the potential for improved retrievals from hyperspectral measurements, J. Geophys. Res.-Atmos., 117, D15206, doi:10.1029/2012JD017896, 2012. 335
Kobayashi, T.: Effects due to cloud geometry on biases in the albedo derived from radiance measurements, J. Climate, 6, 120–128, doi:10.1175/1520-0442(1993)006<0120:EDTCGO>2.0.CO;2, 1993. 309
Liang, L. and Girolamo, L. D.: A global analysis on the view-angle dependence of plane-parallel oceanic liquid water cloud optical thickness using data synergy from MISR and MODIS, J. Geophys. Res.-Atmos., 118, 2389–2403, doi:10.1029/2012JD018201, 2013. 310, 337
Loeb, N. and Coakley, J.: Inference of marine stratus cloud optical depths from satellite measurements: does 1-D theory apply?, J. Climate, 11, 215–233, doi:10.1175/1520-0442(1998)011<0215:IOMSCO>2.0.CO;2, 1998. 309, 328, 332, 337
Loeb, N. and Davies, R.: Observational evidence of plane parallel model biases: apparent dependence of cloud optical depth on solar zenith angle, J. Geophys. Res.-Atmos., 101, 1621–1634, doi:10.1029/95JD03298, 1996. 309, 328, 337
Loeb, N. and Davies, R.: Angular dependence of observed reflectances: a comparison with plane parallel theory, J. Geophys. Res.-Atmos., 102, 6865–6881, doi:10.1029/96JD03586, 1997. 309, 328, 337
Loeb, N., Varnai, T., and Davies, R.: Effect of cloud inhomogeneities on the solar zenith angle dependence of nadir reflectance, J. Geophys. Res.-Atmos., 102, 9387–9395, doi:10.1029/96JD03719, 1997. 309, 310, 314, 315, 327, 332, 337
Loeb, N., Varnai, T., and Winker, D.: Influence of subpixel-scale cloud-top structure on reflectances from overcast stratiform cloud layers, J. Atmos. Sci., 55, 2960–2973, doi:10.1175/1520-0469(1998)055<2960:IOSSCT>2.0.CO;2, 1998. 337
Maddux, B. C., Ackerman, S. A., and Platnick, S.: Viewing geometry dependencies in MODIS cloud products, J. Atmos. Ocean. Tech., 27, 1519–1528, doi:10.1175/2010JTECHA1432.1, 2010. 322
Marshak, A., Davis, A., Wiscombe, W., and Cahalan, R.: Radiative effects of sub-mean free path liquid water variability observed in stratiform clouds, J. Geophys. Res.-Atmos., 103, 19557–19567, doi:10.1029/98JD01728, 1998. 308

ACPD
14, 303–375, 2014

Marshak, A., Platnick, S., Varnai, T., Wen, G., and Cahalan, R.: Impact of three-dimensional radiative effects on satellite retrievals of cloud droplet sizes, J. Geophys. Res.-Atmos., 111, D09207, doi:10.1029/2005JD006686, 2006. 311

Martin, G., JOHNSON, D., and SPICE, A.: The measurement and parameterization of effective radius of droplets in warm stratocumulus clouds, J. Atmos. Sci., 51, 1823–1842, doi:10.1175/1520-0469(1994)051<1823:TMAPOE>2.0.CO;2, 1994. 341

Miles, N., Verlinde, J., and Clothiaux, E.: Cloud droplet size distributions in low-level stratiform clouds, J. Atmos. Sci., 57, 295–311, doi:10.1175/1520-0469(2000)057<0295:CDSDIL>2.0.CO;2, 2000. 341

Morrison, H., de Boer, G., Feingold, G., Harrington, J., Shupe, M. D., and Sulia, K.: Resilience of persistent Arctic mixed-phase clouds, Nat. Geosci., 5, 11–17, doi:10.1038/NGEO1332, 2012. 320

Mossop, S.: Secondary ice particle-production during rime growth – the effect of drop size distribution and rimer velocity, Q. J. Roy. Meteor. Soc., 111, 1113–1124, doi:10.1002/qj.49711147012, 1985. 345

Nakajima, T. and King, M.: Determination of the optical-thickness and effective particle radius of clouds from reflected solar-radiation measurements.1. Theory, J. Atmos. Sci., 47, 1878–1893, doi:10.1175/1520-0469(1990)047<1878:DOTOTA>2.0.CO;2, 1990. 305, 308, 312

Nakajima, T., Higurashi, A., Kawamoto, K., and Penner, J.: A possible correlation between satellite-derived cloud and aerosol microphysical parameters, Geophys. Res. Lett., 28, 1171–1174, doi:10.1029/2000GL012186, 2001. 306

Nakajima, T. Y., Suzuki, K., and Stephens, G. L.: Droplet growth in warm water clouds observed by the A-Train – Part 1: Sensitivity analysis of the MODIS-derived cloud droplet sizes, J. Atmos. Sci., 67, 1884–1896, doi:10.1175/2009JAS3280.1, 2010a. 335

Nakajima, T. Y., Suzuki, K., and Stephens, G. L.: Droplet growth in warm water clouds observed by the A-Train – Part 2: A multisensor view, J. Atmos. Sci., 67, 1897–1907, doi:10.1175/2010JAS3276.1, 2010b. 335

O'Dell, C. W., Wentz, F. J., and Bennartz, R.: Cloud liquid water path from satellite-based passive microwave observations: a new climatology over the global oceans, J. Climate, 21, 1721–1739, doi:10.1175/2007JCLI1958.1, 2008. 325, 326, 336, 343

Oreopoulos, L.: The impact of subsampling on MODIS Level-3 statistics of cloud optical thickness and effective radius, IEEE T. Geosci. Remote, 43, 366–373, doi:10.1109/TGRS.2004.841247, 2005. 318, 319

ACPD
14, 303–375, 2014

Painemal, D. and Zuidema, P.: Assessment of MODIS cloud effective radius and optical thickness retrievals over the Southeast Pacific with VOCALS-REx in situ measurements, J. Geophys. Res.-Atmos., 116, D24206, doi:10.1029/2011JD016155, 2011. 340

Platnick, S.: Vertical photon transport in cloud remote sensing problems, J. Geophys. Res.-Atmos., 105, 22919–22935, doi:10.1029/2000JD900333, 2000. 313, 324, 328, 335

Platnick, S., King, M., Ackerman, S., Menzel, W., Baum, B., Riedi, J., and Frey, R.: The MODIS cloud products: algorithms and examples from Terra, IEEE T. Geosci. Remote, 41, 459–473, doi:10.1109/TGRS.2002.808301, 2003. 305

Quaas, J., Boucher, O., Bellouin, N., and Kinne, S.: Satellite-based estimate of the direct and indirect aerosol climate forcing, J. Geophys. Res.-Atmos., 113, D05204, doi:10.1029/2007JD008962, 2008. 306

Quaas, J., Ming, Y., Menon, S., Takemura, T., Wang, M., Penner, J. E., Gettelman, A., Lohmann, U., Bellouin, N., Boucher, O., Sayer, A. M., Thomas, G. E., McComiskey, A., Feingold, G., Hoose, C., Kristjánsson, J. E., Liu, X., Balkanski, Y., Donner, L. J., Ginoux, P. A., Stier, P., Grandey, B., Feichter, J., Sednev, I., Bauer, S. E., Koch, D., Grainger, R. G., Kirkevåg, A., Iversen, T., Seland, Ø., Easter, R., Ghan, S. J., Rasch, P. J., Morrison, H., Lamarque, J.-F., Iacono, M. J., Kinne, S., and Schulz, M.: Aerosol indirect effects – general circulation model intercomparison and evaluation with satellite data, Atmos. Chem. Phys., 9, 8697–8717, doi:10.5194/acp-9-8697-2009, 2009. 306

Saunders, C. and Hosseini, A.: A laboratory study of the effect of velocity on Hallett-Mossop ice crystal multiplication, Atmos. Res., 59, 3–14, doi:10.1016/S0169-8095(01)00106-5, 13th International Conference on Clouds and Precipitation, Desert Res Inst, Reno, Nevada, 14–17 August, 2000, 2001. 345

Seethala, C. and Horvath, A.: Global assessment of AMSR-E and MODIS cloud liquid water path retrievals in warm oceanic clouds, J. Geophys. Res.-Atmos., 115, D13202, doi:10.1029/2009JD012662, 2010. 311, 315, 324, 335

Shupe, M. D.: Clouds at Arctic atmospheric observatories – Part 2: Thermodynamic phase characteristics, J. Appl. Meteorol. Clim., 50, 645–661, doi:10.1175/2010JAMC2468.1, 2011. 343

Tjernstrom, M.: Is there a diurnal cycle in the summer cloud-capped arctic boundary layer?, J. Atmos. Sci., 64, 3970–3986, doi:10.1175/2007JAS2257.1, 2007. 343

ACPD
14, 303–375, 2014

Varnai, T. and Davies, R.: Effects of cloud heterogeneities on shortwave radiation: comparison of cloud-top variability and internal heterogeneity, J. Atmos. Sci., 56, 4206–4224, doi:10.1175/1520-0469(1999)056<4206:EOCHOS>2.0.CO;2, 1999. 309, 310, 315, 327, 337
Wood, R.: Drizzle in stratiform boundary layer clouds – Part 1: Vertical and horizontal structure, J. Atmos. Sci., 62, 3011–3033, doi:10.1175/JAS3529.1, 2005a. 341
Wood, R.: Drizzle in stratiform boundary layer clouds – Part 1: Vertical and horizontal structure, J. Atmos. Sci., 62, 3011–3033, doi:10.1175/JAS3529.1, 2005b. 341
Wood, R.: Rate of loss of cloud droplets by coalescence in warm clouds, J. Geophys. Res.-Atmos., 111, D21205, doi:10.1029/2006JD007553, 2006. 342
Wood, R.: Stratocumulus clouds, Mon. Weather Rev., 140, 2373–2423, doi:10.1175/MWR-D-11-00121.1, 2012. 342
Wood, R. and Hartmann, D.: Spatial variability of liquid water path in marine low cloud: the importance of mesoscale cellular convection, J. Climate, 19, 1748–1764, doi:10.1175/JCLI3702.1, 2006. 314
Wood, R., Bretherton, C. S., and Hartmann, D. L.: Diurnal cycle of liquid water path over the subtropical and tropical oceans, Geophys. Res. Lett., 29, 7-1–7-4, doi:10.1029/2002GL015371, 2002. 343
Wood, R., Leon, D., Lebsock, M., Snider, J., and Clarke, A. D.: Precipitation driving of droplet concentration variability in marine low clouds, J. Geophys. Res.-Atmos., 117, D19210, doi:10.1029/2012JD018305, 2012. 306, 342
Zhang, Z.: On the sensitivity of cloud effective radius retrieval based on spectral method to bi-modal droplet size distribution: a semi-analytical model, J. Quant. Spectrosc. Ra., 129, 79–88, doi:10.1016/j.jqsrt.2013.05.033, 2013. 332, 334, 358
Zhang, Z. and Plantnick, S.: An assessment of differences between cloud effective particle radius retrievals for marine water clouds from three MODIS spectral bands, J. Geophys. Res.-Atmos., 116, D20215, doi:10.1029/2011JD016216, 2011. 314, 324, 328
Zhang, Z., Ackerman, A. S., Feingold, G., Platnick, S., Pincus, R., and Xue, H.: Effects of cloud horizontal inhomogeneity and drizzle on remote sensing of cloud droplet effective radius: case studies based on large-eddy simulations, J. Geophys. Res.-Atmos., 117, D19208, doi:10.1029/2012JD017655, 2012. 308
Zinner, T., Wind, G., Platnick, S., and Ackerman, A. S.: Testing remote sensing on artificial observations: impact of drizzle and 3-D cloud structure on effective radius retrievals, Atmos. Chem. Phys., 10, 9535–9549, doi:10.5194/acp-10-9535-2010, 2010. 335

ACPD
14, 303–375, 2014

Zuidema, P., Westwater, E., Fairall, C., and Hazen, D.: Ship-based liquid water path estimates in marine stratocumulus, J. Geophys. Res.-Atmos., 110, D20206, doi:10.1029/2005JD005833, 2005. 341

ACPD
14, 303–375, 2014

Table 1. Various parameters for different subsets of the dataset for which various restrictions have been applied. Low θ: $0 < \theta \leq 41.4^{\circ}$; high θ: $\theta > 41.4^{\circ}$; low θ_0: $50 < \theta_0 \leq 55^{\circ}$; high θ_0: $\theta_0 > 75^{\circ}$; low σ_{CTT}: $\sigma_{CTT} \leq 0.65$ K; high σ_{CTT}: $\sigma_{CTT} > 1$ K.

		2.1 μm						1.6 μm					3.7 μm				
Data subset	$\overline{\tau}$	σ_{τ} (%)	$\overline{r_e}$ (μm)	σ_{r_e} (%)	$\overline{N_d}$ (cm^{-3})	σ_{N_d} (%)	$r_{\tau,re}$	$\overline{r_e}$ (μm)	σ_{r_e} (%)	$\overline{N_d}$ (cm^{-3})	σ_{N_d} (%)	$r_{\tau,re}$	$\overline{r_e}$ (μm)	σ_{r_e} (%)	$\overline{N_d}$ (cm^{-3})	σ_{N_d} (%)	$r_{\tau,re}$
Low θ, low θ_0	16.4	47.4	12.1	15.8	104.1	47.2	0.03	12.2	15.7	100.8	43.7	0.13	12.2	17.9	107.1	59.6	0.00
Low θ, high θ_0	27.9	53.0	11.5	16.7	154.3	50.8	−0.01	12.0	17.2	140.2	54.2	−0.18	11.3	16.9	161.9	52.1	0.15
High θ, low θ_0	16.8	47.0	12.7	15.5	92.9	48.5	0.05	12.6	15.9	93.6	47.1	0.11	12.5	16.6	97.5	54.2	0.05
High θ, high θ_0	32.3	55.9	11.7	16.3	153.5	45.8	0.18	12.4	16.5	137.4	57.8	−0.15	11.4	18.5	163.8	48.3	0.37
Low σ_{CTT}, low θ_0	17.0	44.3	12.6	15.5	94.6	45.2	0.04	12.4	16.1	97.9	43.6	0.15	13.1	16.0	88.5	54.7	0.07
Low σ_{CTT}, high θ_0	30.4	50.7	11.9	15.8	146.9	48.8	−0.10	12.2	17.2	142.7	52.4	−0.22	11.8	15.3	146.8	47.0	0.09
High σ_{CTT}, low θ_0	16.5	51.8	11.4	14.3	118.2	45.9	−0.02	11.8	14.4	107.1	42.5	0.10	11.1	16.3	132.5	55.4	−0.12
High σ_{CTT}, high θ_0	24.8	52.8	10.5	16.1	184.8	54.6	−0.10	11.6	16.5	146.7	59.1	−0.18	9.9	15.9	213.7	52.3	−0.00

ACPD
14, 303–375, 2014

Table 2. Changes in various quantities between the lowest and highest θ_0 bins (high minus low). Four different data subsets are shown with parameter ranges as for Table 1. For "All σ_{CTT}" there were no restrictions on σ_{CTT}.

		2.1 µm						1.6 µm						3.7 µm					
Data subset	$\Delta\tau$ (%)	ΔNd (%)	ΔRe (%)	$\Delta N_{\Delta\tau}$ (%)	$\Delta N_{\Delta re}$ (%)	$t_{\Delta\tau}$	$t_{\Delta re}$	ΔNd (%)	ΔRe (%)	$\Delta N_{\Delta\tau}$ (%)	$\Delta N_{\Delta re}$ (%)	$t_{\Delta\tau}$	$t_{\Delta re}$	ΔNd (%)	ΔRe (%)	$\Delta N_{\Delta\tau}$ (%)	$\Delta N_{\Delta re}$ (%)	$t_{\Delta\tau}$	$t_{\Delta re}$
All σ_{CTT}, low θ	69.8	48.3	−4.8	29.26	14.24	1.09	1.11	39.1	−1.1	29.20	4.99	1.08	1.11	51.2	−7.4	29.27	20.34	1.08	1.11
All σ_{CTT}, high θ	92.4	65.3	−8.0	37.36	23.83	1.09	1.11	46.8	−1.6	37.34	4.67	1.09	1.11	67.9	−8.7	37.28	30.14	1.09	1.11
Low σ_{CTT}, low θ	79.1	55.2	−5.7	32.54	15.86	1.09	1.09	45.8	−2.2	32.58	7.46	1.09	1.11	65.8	−9.5	32.55	27.21	1.09	1.11
High σ_{CTT}, low θ	49.7	56.4	−8.0	22.25	26.10	1.07	1.10	36.9	−2.1	22.28	9.13	1.07	1.10	61.3	−10.7	22.32	34.45	1.07	1.10

ACPD
14, 303–375, 2014

Table 3. Summary of possible factors that cause changes in r_e with θ_0.

Effect	Sign of effect on r_e for high θ_0 minus low θ_0 retrievals	Reference	Band dependence	Comments
(1) The averaging scale effect:–				Caused by the non-linearity of the $R_{ab} - r_e$ relationship.
Small averaging scales	+ve	M06	Increase greater for 3.7 µm than 2.1 µm.	Less increase expected for low θ_0 due to fewer 3-D effects.
Large averaging scales	–ve	M06 & Z12	Likely that the reduction in r_e with θ_0 larger for 2.1 µm than 3.7 µm.	3-D effects start to cancel out and the sub-pixel positive bias of Z12 likely dominates.
(2) Plane-parallel (PP) re bias	–ve	See Sect. 2.2.1	Unknown	Caused by 3-D radiative transfer increasing the upwards photon flux of real clouds relative to PP clouds – photon interception by sides, tilted cloud tops (increased effective cloud fraction), etc.
(3) Droplet size distibution (DSD) width	Unknown	Zhang (2013)	Reduction at low θ_0 greater for 3.7 µm than 2.1 µm.	In heterogeneous clouds the DSD is likely to be wider than that assumed by MODIS, which causes a negative bias at low θ_0. The high θ_0 effect unknown.

ACPD
14, 303–375, 2014

Table 4. Results from the example calculations of 3D radiative effects at small averaging scales, as demonstrated in Fig. 14, except that results from various other view angles (θ) and relative azimuth angles (ϕ) are also shown. 3-D effects at high θ_0 are assumed to cause an equal increase and decrease (ΔR) in the reflectances of both the absorbing band (R_{ab}) and the non-absorbing band (R_{nab}). For this demonstration it is assumed that there are an equal number of small scale cloud elements all with r_e = 14 µm and τ = 23.6. Retrievals are then made on the reflectances that have been distorted by the 3-D effects using MODIS lookup tables (LUTs) that are used for converting non-absorbing (0.86 µm) and absorbing reflectance pairs into τ and r_e. These are shown for $\theta_0 = 79^\circ$ and for the 1.6 µm, 2.1 µm and 3.7 µm absorbing bands. It can be seen that in all cases the retrieved r_e would be greater than the true r_e of 14 µm. See Sect. 4.1 for further details.

θ	ϕ	Band	Retrieved r_e	Difference from true r_e
0°	N/A	1.6 µm	14.7	0.7
0°	N/A	2.1 µm	15.3	1.3
0°	N/A	3.7 µm	19.3	5.3
50°	30°	1.6 µm	14.1	0.1
50°	30°	2.1 µm	14.3	0.3
50°	30°	3.7 µm	14.4	0.4
50°	150°	1.6 µm	14.3	0.3
50°	150°	2.1 µm	14.7	0.7
50°	150°	3.7 µm	15.5	1.5

ACPD
14, 303–375, 2014

Table A1. As for Table 1 except for parameters relevant for the Latin Hypercube Sampling sensitivity analysis (see text for details).

Data subset	2.1 µm		1.6 µm		3.7 µm	
	w	s_{lhs}	w	s_{lhs}	w	s_{lhs}
Low θ, low θ_0	1.09	1.02	1.09	1.02	1.13	1.00
Low θ, high θ_0	1.10	1.01	1.10	1.00	1.11	1.03
High θ, low θ_0	1.10	1.03	1.10	1.03	1.11	1.02
High θ, high θ_0	1.09	1.05	1.09	1.01	1.15	1.09
Low σ_{CTT}, low θ_0	1.09	1.02	1.10	1.02	1.11	1.01
Low σ_{CTT}, high θ_0	1.09	1.01	1.10	1.00	1.09	1.03
High σ_{CTT}, low θ_0	1.07	1.01	1.07	1.02	1.09	0.99
High σ_{CTT}, high θ_0	1.09	1.00	1.10	0.99	1.10	1.01

ACPD
14, 303–375, 2014

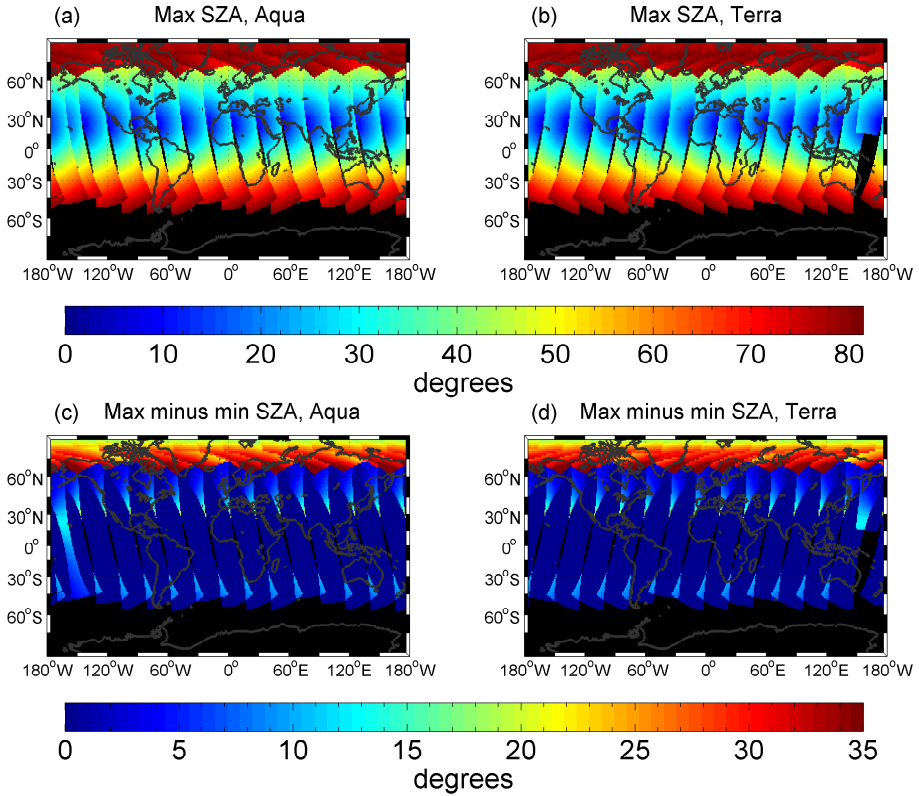

Fig. 1. Solar Zenith Angle (θ_0) properties for a single day (20th June 2007; approximately the solstice) of maximum θ_0 (**a** and **b**) and maximum minus minimum θ_0 (**c** and **d**) for daytime (SZA $\leq 81.4^{\circ}$) data. (**a** and **c**) MODIS Aqua, (**b** and **d**) MODIS Terra.

ACPD
14, 303–375, 2014

MODIS cloud optical and microphysical retrievals

D. P. Grosvenor and R. Wood

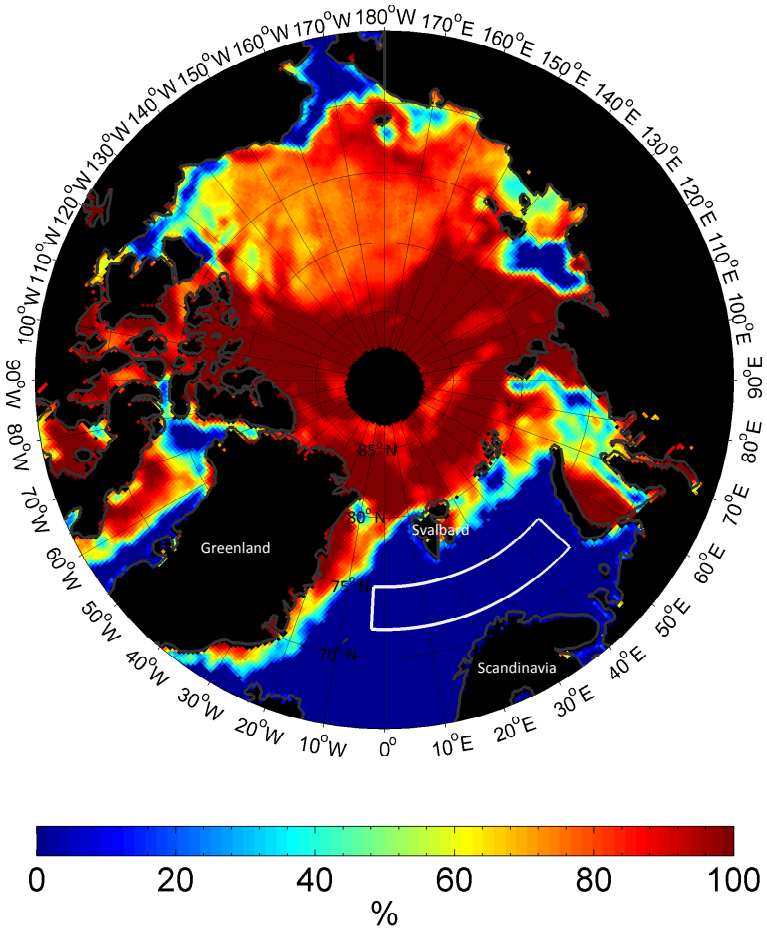

Fig. 2. The region of interest for this study (white box; 72 to 75° N, −3 to 48° E) plotted onto a map of sea-ice areal coverage (%) for 13 June 2007, which was the start of the studied period. Sea ice generally was diminishing with time throughout the period.

ACPD
14, 303–375, 2014

MODIS cloud optical and microphysical retrievals

D. P. Grosvenor and R. Wood

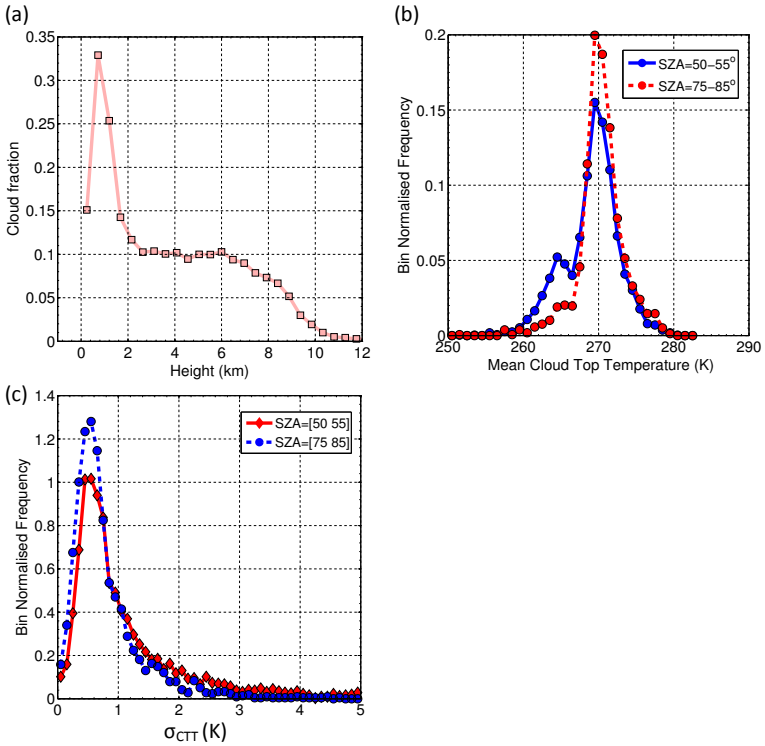

Fig. 3. (a) CALIPSO cloud fraction vs. height for the month of June for the years 2007–2010. **(b)** PDFs of mean MODIS gridbox cloud top temperature (CTT) for gridboxes containing liquid clouds only (restrictions 1–4 applied, see text) and for $\theta \leq 41.4^{\circ}$. The difference between the low and high θ_0 PDFs is highly likely to be due to phase determination problems at high θ_0 (see text for explanation). When considering clouds of all phases the PDFs are identical (not shown). **(c)** PDFs of the standard deviation of CTT within gridboxes for datapoints that have had restrictions (1–5) applied (see text) and for $\theta \leq 41.4^{\circ}$.

ACPD
14, 303–375, 2014

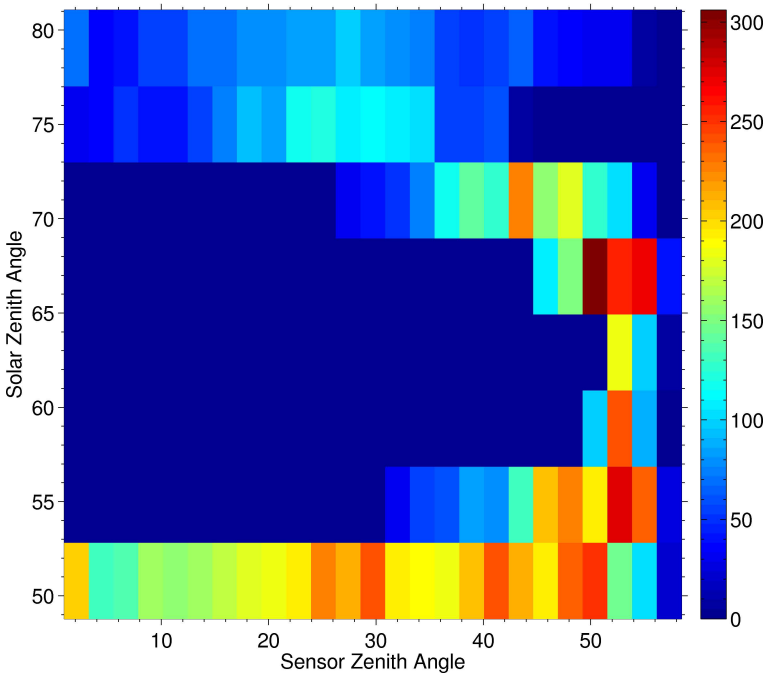

Fig. 4. 2-D histogram of solar zenith angle vs. sensor zenith angle for the $1^{\circ} \times 1^{\circ}$ grid boxes used as datapoints in this study. The colours represent the number of such datapoints at each pairing. Data has been filtered according to the criteria outlined in the text.

ACPD
14, 303–375, 2014

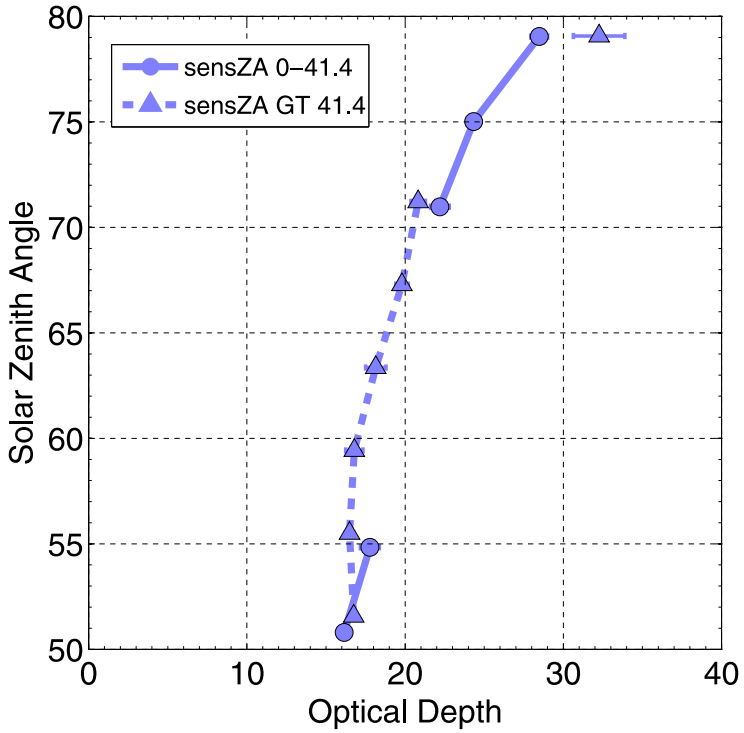

Fig. 5. Mean optical depth vs. solar zenith angle for different ranges of sensor zenith angle (see legend: $\theta > 41.4$ and $0 < \theta \leq 41.4$).

ACPD
14, 303–375, 2014

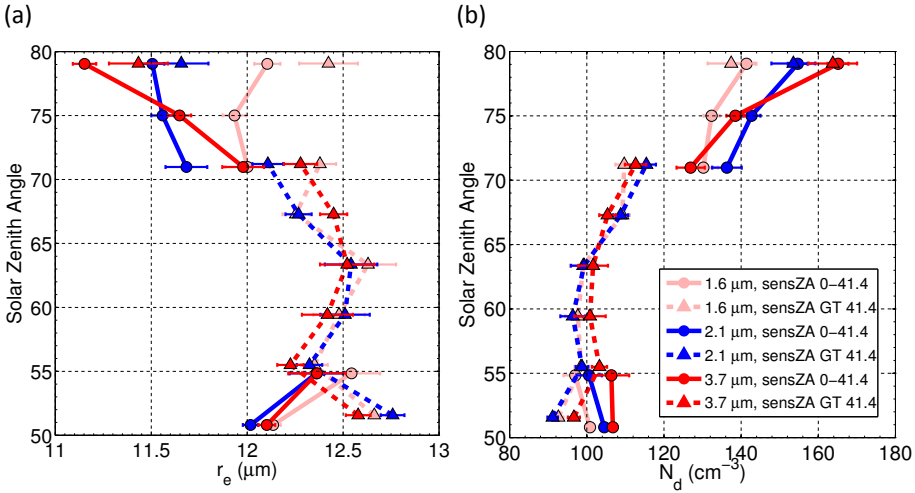

Fig. 6. As for Fig. 5 except for the mean effective radius **(a)** and droplet concentration **(b)** for the different MODIS bands.

ACPD
14, 303–375, 2014

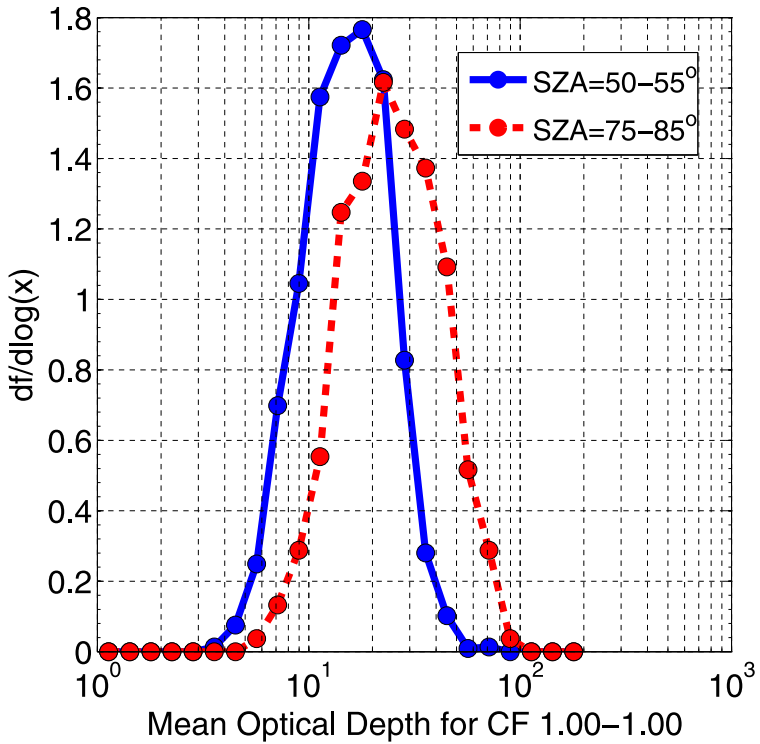

Fig. 7. PDFs of optical depth (τ) for low sensor zenith angles ($0 > \theta \leq 41.4$) and for different Solar Zenith Angles (SZA or θ_0, see the legend). Other data restrictions are described in the text. Probabilities are normalized by the bin widths in $\log_{10}$ space.

ACPD
14, 303–375, 2014

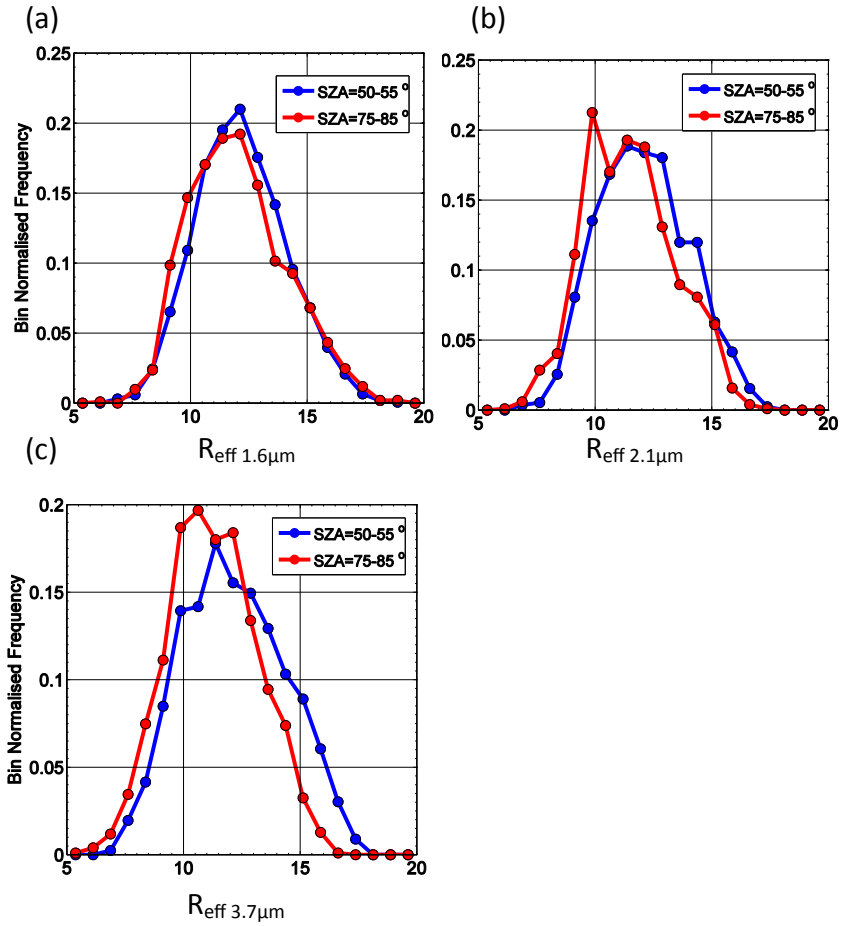

Fig. 8. As for Fig. 7 except for r_e and that the probabilities are normalized by the bin widths in linear space. Results are shown for the three different MODIS bands.

ACPD
14, 303–375, 2014

MODIS cloud optical and microphysical retrievals

D. P. Grosvenor and R. Wood

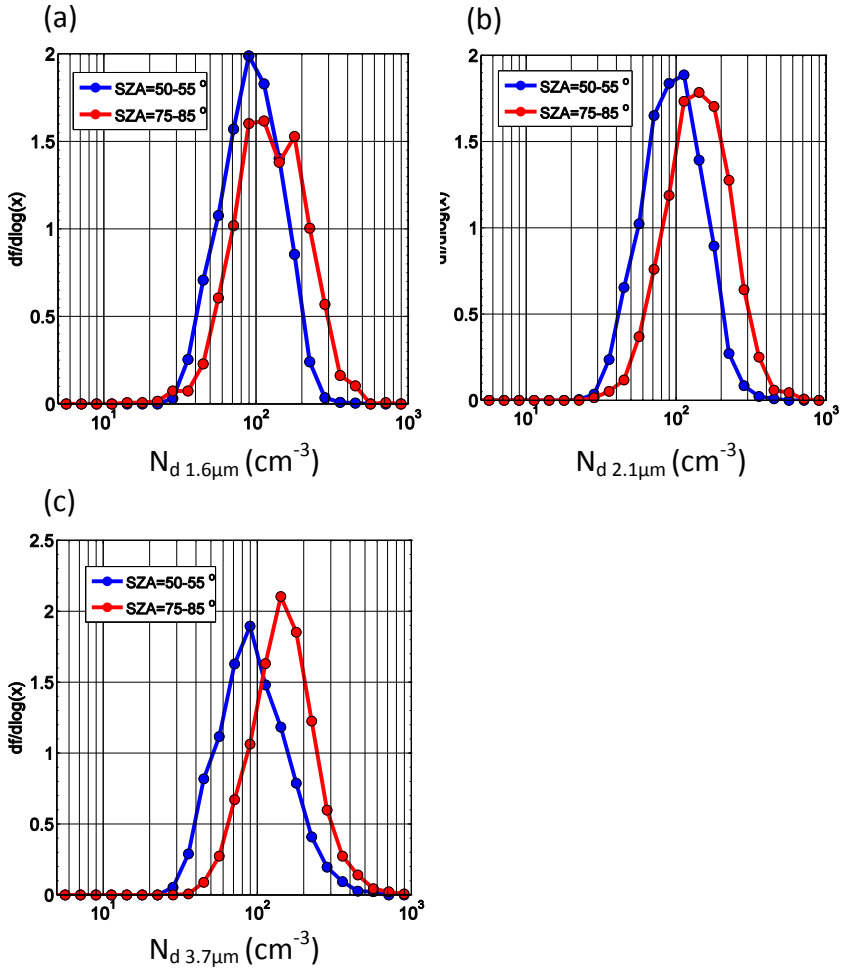

Fig. 9. As for Fig. 8 except for N_d.

ACPD
14, 303–375, 2014

MODIS cloud optical and microphysical retrievals

D. P. Grosvenor and R. Wood

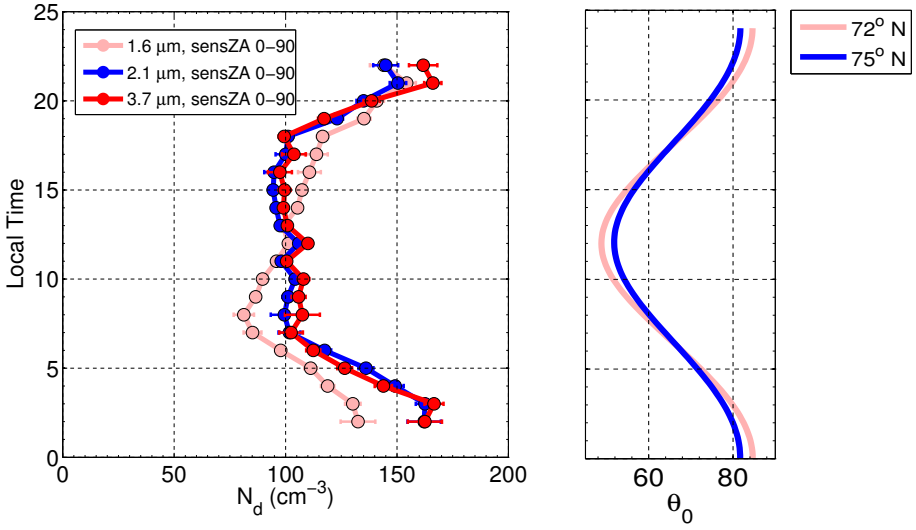

Fig. 10. N_d and θ_0 (right panel) vs. local time of day. For the $r_{e2.1}$ and $r_{e3.7}$ based N_d retrievals, the flatness of the curves for the times corresponding to lower θ_0 suggests that there is little physical diurnal cycle of N_d. This suggests that the changes seen at high θ_0 are the result of retrieval artifacts and not physical effects. All θ values are included and N_d values are shown for retrievals made using $r_{e1.6}$, $r_{e2.1}$ and $r_{e3.7}$. For the θ_0 plot, values are shown at the most southern (72° N) and northern (75° N) edges of the region. Over the period of study, time variation of θ_0 from day to day was very slight for a given local time and gridbox.

ACPD
14, 303–375, 2014

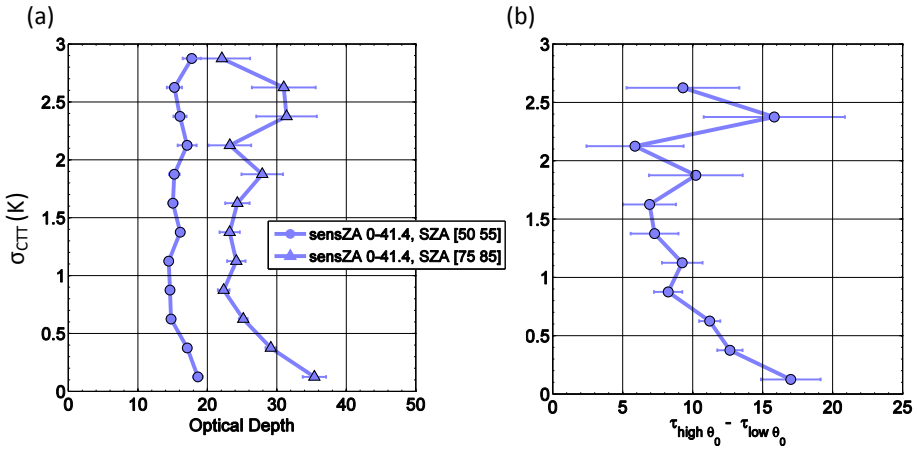

Fig. 11. Optical depth vs. σ_{CTT} for low sensor zenith angles ($0 < \theta \leq 41.4$) and for different Solar Zenith Angles (SZA or θ_0, see the legend). Other data restrictions are described in the text.

ACPD
14, 303–375, 2014

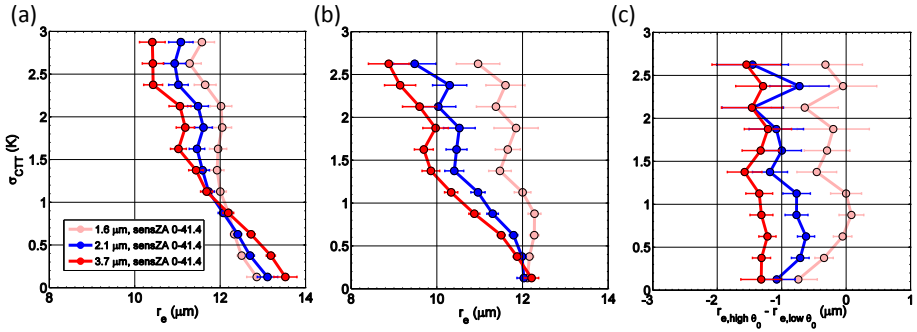

Fig. 12. As for Fig. 11 except for effective radius for low θ_0 **(a)**, high θ_0 **(b)**, and the difference between r_e at high and low θ_0 **(c)**.

ACPD
14, 303–375, 2014

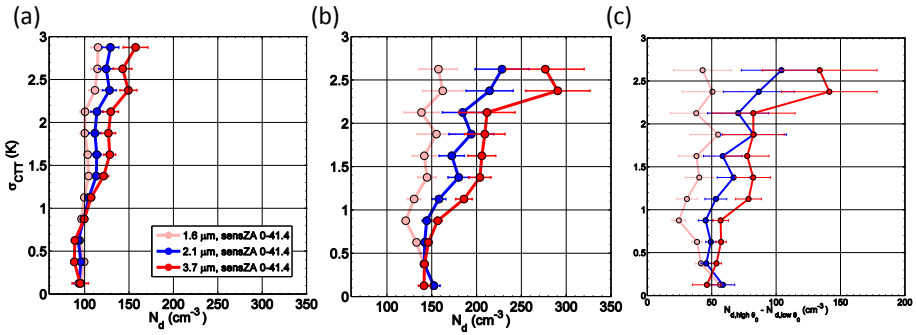

Fig. 13. As for Fig. 12 except for droplet number concentration.

ACPD
14, 303–375, 2014

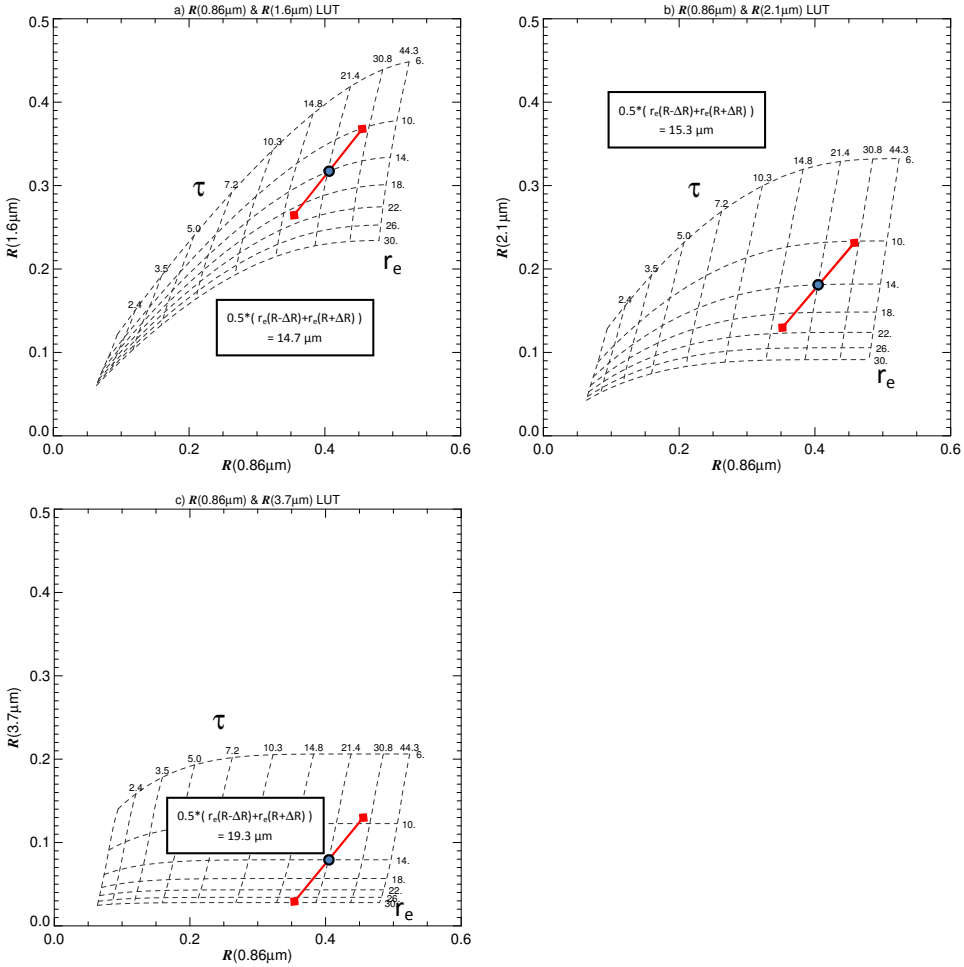

ACPD
14, 303–375, 2014

MODIS cloud optical and microphysical retrievals

D. P. Grosvenor and R. Wood

Fig. 14. An example of the effect of 3-D effects on MODIS retrievals at small averaging scales. 3-D effects at high θ_0 are assumed to cause an equal increase and decrease (ΔR) in the reflectances of both the absorbing band (R_{ab}) and the non-absorbing band (R_{nab}). For this demonstration it is assumed that there are an equal number of small scale cloud elements all with r_e = 14 µm and τ = 23.6. Retrievals are then made on the reflectances that have been distorted by the 3-D effects using MODIS lookup tables (LUTs) that are used for converting non-absorbing (0.86 µm) and absorbing reflectance pairs into τ and r_e. These are shown for $\theta_0 = 79^\circ$ and a nadir viewing angle. **(a)** is for the 1.6 µm absorbing band, **(b)** for 2.1 µm and **(c)** for 3.7 µm. It can be seen that in all cases the retrieved r_e would be greater than the true r_e of 14 µm. See Sect. 4.1 for further details.

ACPD
14, 303–375, 2014